ICM IN THE MM

Credits: L. Di Mascolo, A. Saro

For a review: https://arxiv.org/pdf/astro-ph/9808050

THE tSZ EFFECT

Sunyaev-Zel'dovich effect (1970):

- **Inverse compton scattering of low energy CMB photons with free electrons in the hot ICM.**
- **Each scattering changes the frequency of the photon, and up-scattering is more likely:**

$$\Delta\nu/\nu \simeq k_B T_e / m_e c^2 \sim 10^{-2}$$

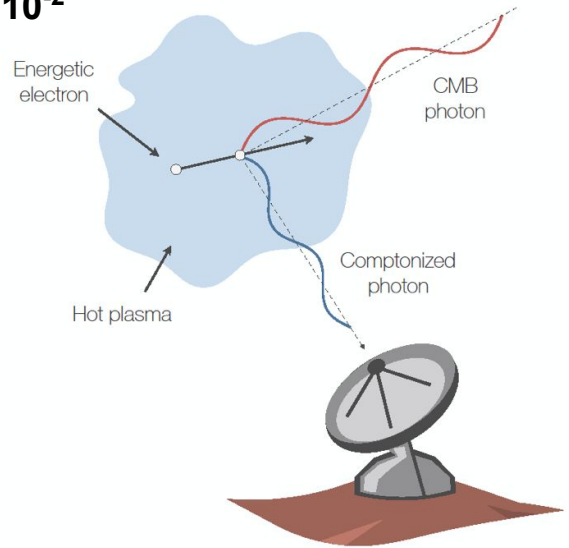

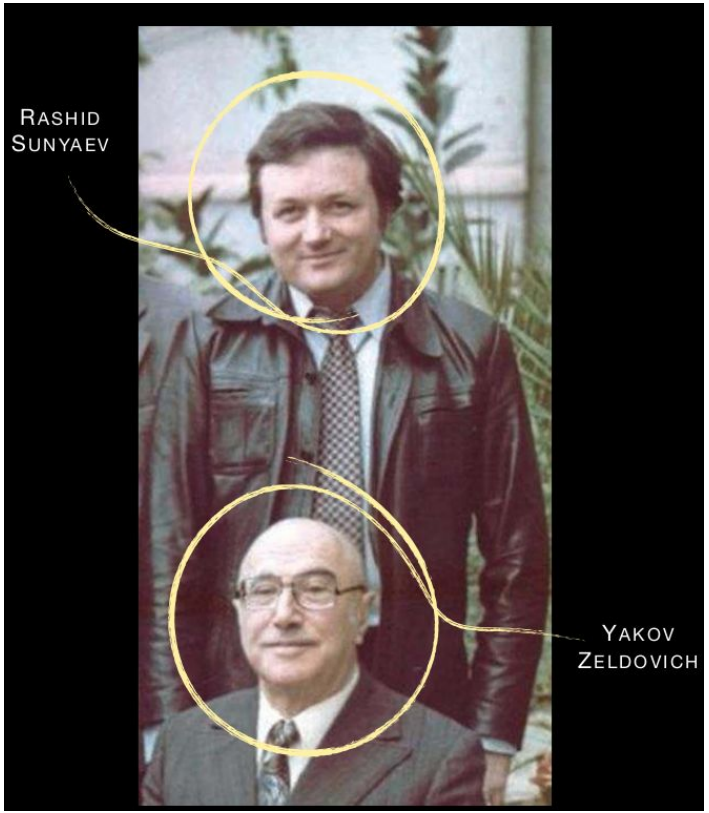

THE tSZ EFFECT

Sunyaev-Zel'dovich effect (1972):

The Observation of Relic Radiation as a Test of the Nature of X-Ray Radiation from the Clusters of Galaxies

Introduction

The x-ray radiation from a number of clusters of galaxies (Coma, Virgo, Perseus) was discovered recently.[1] It is assumed that clusters of galaxies form an important class of powerful x-ray sources, possibly giving the main contribution to the x-ray background radiation of the Universe.[2] What is the nature of these sources? What physical mechanisms give the observed x-ray radiation?

If hot intergalactic gas really exists in clusters of galaxies, there are all the conditions for action of the proposed effect. Thus, for example, the x-ray radiation of the Coma cluster of galaxies is interpreted as the bremsstrahlung radiation of a hot intergalactic gas having $T_e \sim 7 \times 10^7$ °K and the density $N_e \sim 10^{-3}$ cm^{-3}. The linear dimension of the source is estimated to be $l \sim 10^{25}$ cm^{-3}. Multiplying these figures, we find

$$\frac{\Delta T_r}{T_r} = -2y = -2\sigma_T N_e l \frac{kT_e}{m_e c^2} \sim 2 \times 10^{-4},$$

the value accessible for observations. Namely, such effect was recently discovered in Coma by Pariysky.[11]

The deficit of brightness (hole) in the Coma is difficult to understand by any other mechanism! The radiation temperature is 2.7 °K; an arbitrary absorption

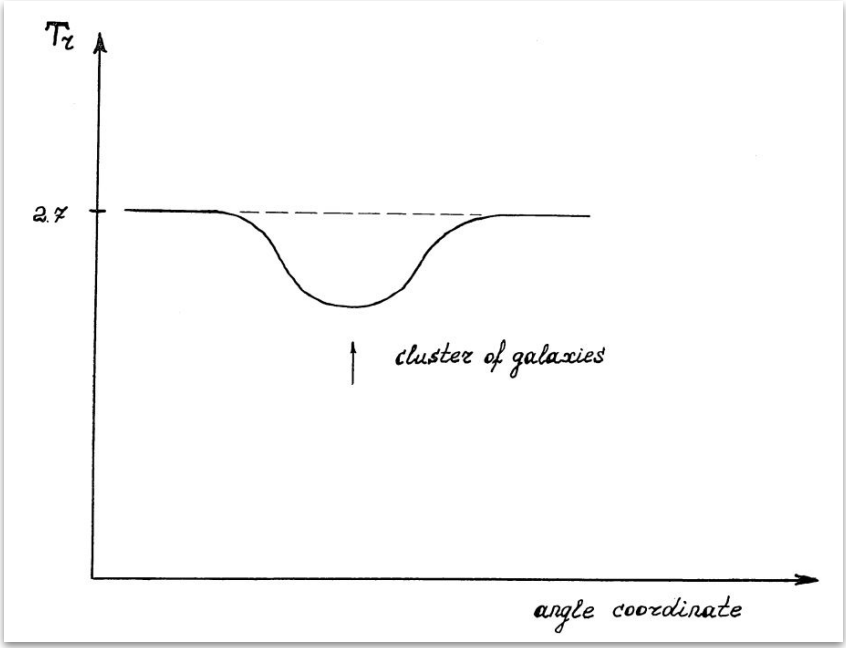

THE tSZ EFFECT

Sunyaev-Zel'dovich effect (1970):

- **Inverse compton scattering of low energy CMB photons with free electrons in the hot ICM.**
- **Each scattering changes the frequency of the photon, and up-scattering is more likely:**

$$\Delta\nu/\nu \approx k_B T_e / m_e c^2 \sim 10^{-2}$$

- **The net effect is a distortion of the CMB black body spectrum → low energy photons are up-scattered to higher frequencies inducing a characteristic spectral signature**

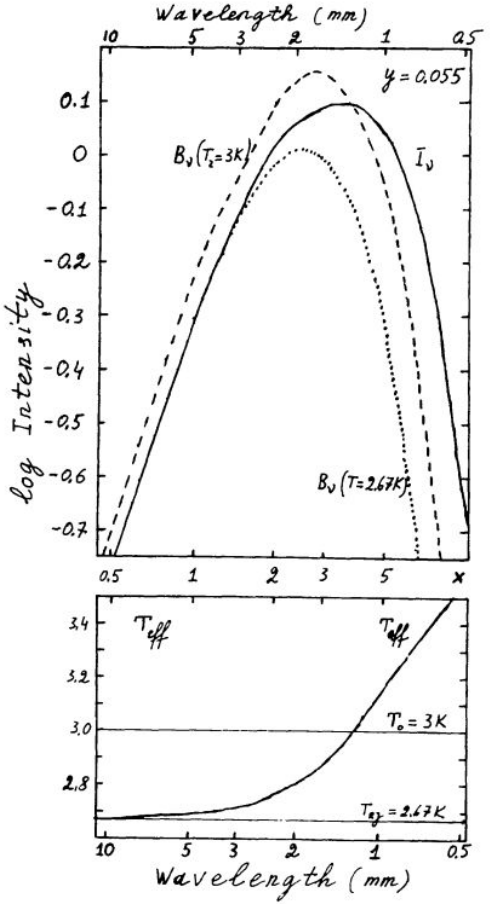

THE tSZ EFFECT

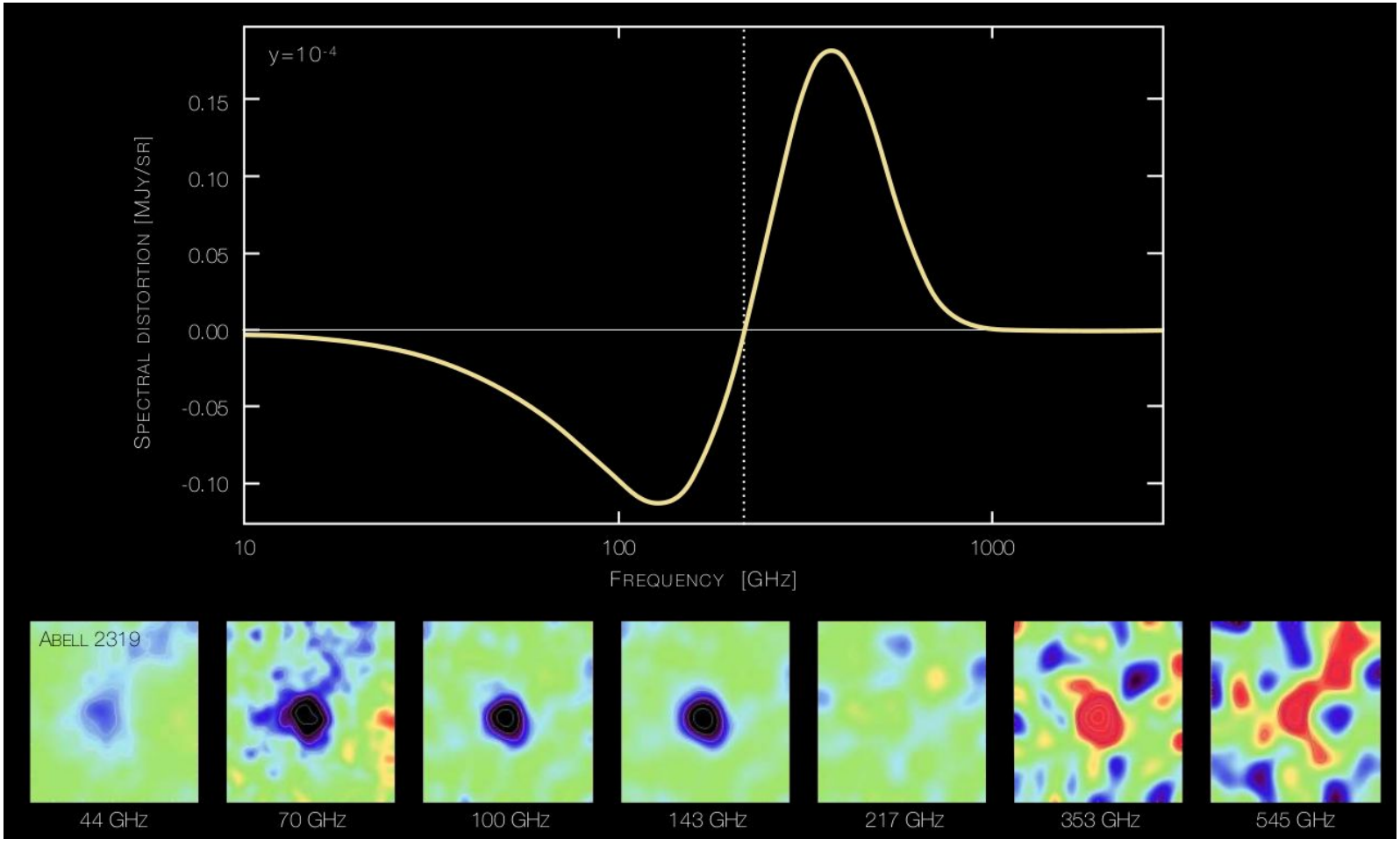

THE tSZ EFFECT

The tSZ spectral distortion:

$$\delta I_\nu \approx \frac{2(k_\mathrm{B}T_\mathrm{CMB})^3}{(h\nu)^2}\frac{x^4e^x}{(e^x-1)^2}\left[x\frac{e^x+1}{e^x-1}-4\right]y$$

$$\delta T \approx T_\mathrm{CMB}\left[x\frac{e^x+1}{e^x-1}-4\right]y$$

Amplitude

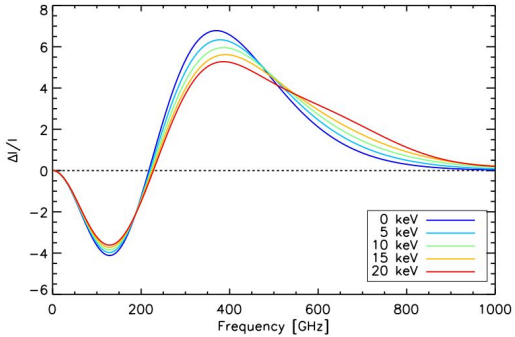

Compton-y parameter:

$$y = \frac{\sigma_\mathrm{T}}{m_e c^2}\int n_e T_e dl$$

Electron pressure

Spectral signature:
- **Negative at low frequencies**
- **Positive at high frequencies**
- **Transition at x ≃ 3.83 → ν ≃ 220 GHz**

Reduced frequency:

$$x = \frac{h\nu}{k_\mathrm{B}T_\mathrm{CMB}}$$

THE tSZ EFFECT

The tSZ spectral distortion:

$$\delta I_\nu \approx \frac{2(k_B T_{CMB})^3}{(h\nu)^2} \frac{x^4 e^x}{(e^x-1)^2} \left[x \frac{e^x+1}{e^x-1} - 4 \right] y$$

$$\delta T \approx T_{CMB} \left[x \frac{e^x+1}{e^x-1} - 4 \right] y$$

→ **Spectral distortion independent from the cluster redshift**

Compton-y parameter:

$$y = \frac{\sigma_T}{m_e c^2} \int n_e T_e dl$$

~Redshift independent!

Reduced frequency:

$$x = \frac{h\nu}{k_B T_{CMB}} = \frac{h[\nu_0(1+z)]}{k_B[T_0(1+z)]} = \frac{h\nu_0}{k_B T_0}$$

Cluster redshift

$T(z)_{CMB}$ assuming adiabatic expansion

Redshift independent!

THE tSZ EFFECT

The tSZ spectral distortion can be used to measure the CMB temperature over cosmic time:

$$x = \frac{h\nu}{k_B T_{CMB}} = \frac{h[\nu_0(1+z)]}{k_B[T_0(1+z)^{1+\beta}]}$$

$$\delta T \simeq T_{CMB} f(x) y$$

Redshift dependent!

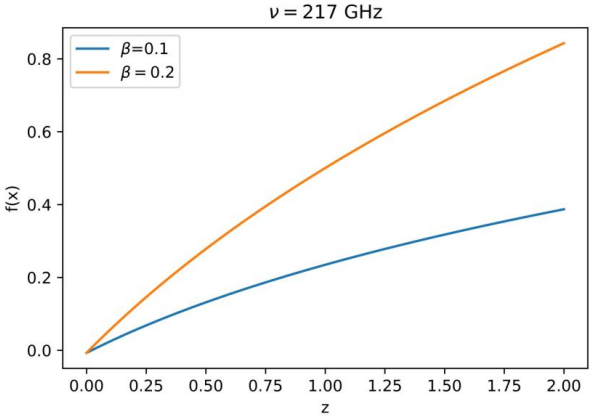

$$\frac{\delta T_{\nu_1}}{\delta T_{\nu_2}} = \frac{f(x_{\nu_1})}{f(x_{\nu_2})}$$

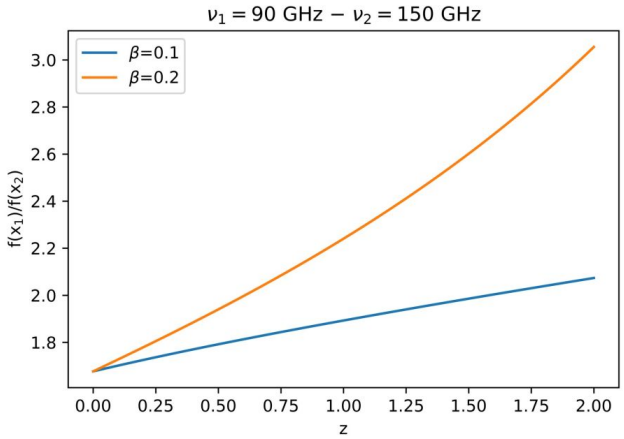

$$\nu_{\mathrm{null}}(z) = x_{\mathrm{null}} \frac{k_b T_0}{h} (1+z)^{\beta}$$

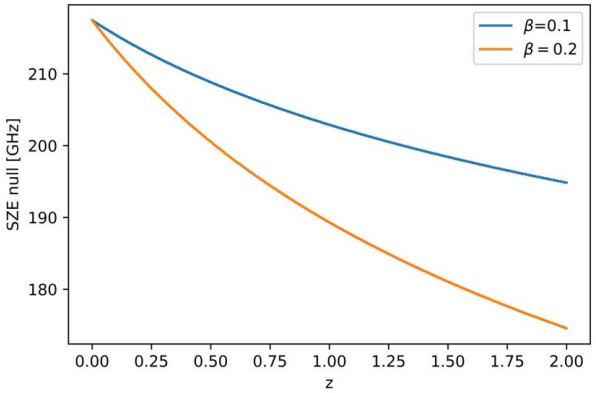

THE tSZ EFFECT

The tSZ spectral distortion can be used to measure the CMB temperature over cosmic time:

Avgoustidis et al. 2016

Method	Reference	z	N	$T_{\rm CMB}$ (K)	β	Label
SZ effect towards clusters	Saro et al. (2014) [18]	$0.055 - 1.350$	158	-	0.017 ± 0.030	[a]
		$0.3 - 1.350$		-	0.016 ± 0.031	[b]
	de Martino et al. (2015) [15]	< 0.3	481	-	-0.007 ± 0.013	[c]
	Luzzi et al. (2015) [16]	$0.011 - 0.972$	103	-	0.012 ± 0.016	[d]
		$0.011 - 0.972$	99	-	0.014 ± 0.016	[e]
		$0.3 - 0.972$	33	-	0.020 ± 0.017	[f]
	Luzzi et al. (2009) [14]	$0.023 - 0.546$	13	-	0.065 ± 0.080	[g]
		$0.200 - 0.546$	7	-	0.044 ± 0.087	[h]
		$0.3 - 0.546$	2	-	0.05 ± 0.14	[i]
	Hurier et al. (2014) [17]	$0 - 1$	813	-	0.009 ± 0.017	[j]
		$0.30 - 0.35$	81	3.562 ± 0.050	-0.006 ± 0.022	[k]
		$0.35 - 0.40$	50	3.717 ± 0.063		
		$0.40 - 0.45$	45	3.971 ± 0.071		
		$0.45 - 0.50$	26	3.943 ± 0.112		
		$0.50 - 0.55$	20	4.380 ± 0.119		
		$0.55 - 0.60$	18	4.075 ± 0.156		
		$0.60 - 0.65$	12	4.404 ± 0.194		
		$0.65 - 0.70$	6	4.779 ± 0.278		
		$0.70 - 0.75$	5	4.933 ± 0.371		
		$0.75 - 0.80$	2	4.515 ± 0.621		
		$0.85 - 0.90$	1	5.356 ± 0.617		
		$0.95 - 1.00$	1	5.813 ± 1.025		
QSO absorption lines	Muller et al. (2013) [19]	0.89	1	$5.0791^{+0.0993}_{-0.0994}$	0.005 ± 0.022	[l]
	Noterdeame et al. (2011) [20]	1.7293	1	$7.5^{+1.6}_{-1.2}$		
		1.7738	1	$7.8^{+0.7}_{-0.6}$		
		2.0377	1	$8.6^{+1.1}_{-1.0}$		
	Cui et al. (2005) [21]	1.77654	1	7.2 ± 0.8		
	Ge et al. (2001) [22]	1.9731	1	7.9 ± 1.0		
	Srianand et al. (2000) [23]	2.33771	1	$6 - 14$		
	Srianand (2008) [24]	2.4184	1	9.15 ± 0.72		
	Noterdaeme et al. (2010) [25]	2.6896	1	$10.5^{+0.8}_{-0.6}$		
	Molaro et al. (2002) [26]	3.025	1	$12.1^{+1.7}_{-3.2}$		

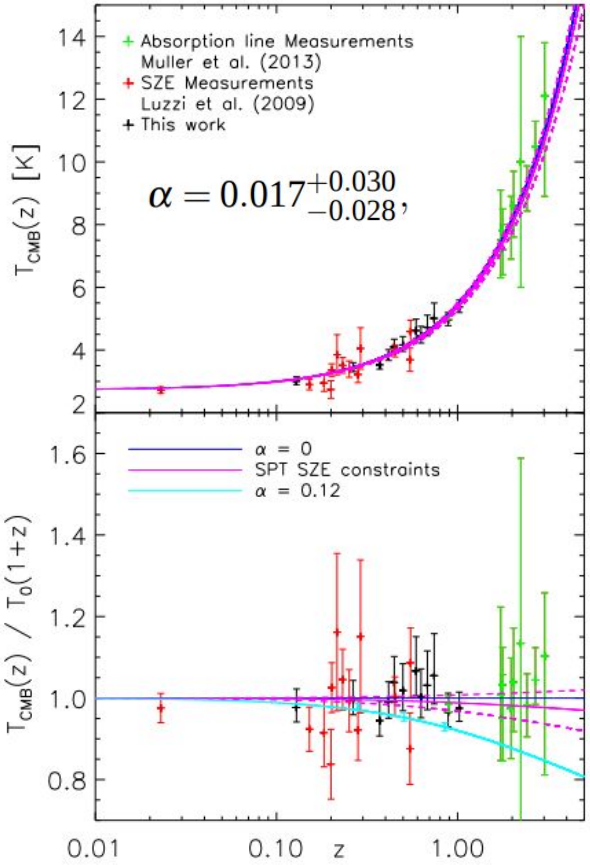

Saro et al. 2014

H_0 FROM X-RAY AND SZ MEASUREMENTS

Based on a distance measuring techniques that depend on a comparison of 2 observables (Cavaliere+77):

$$E \propto \int n_e^2 dl$$

$$A \propto \int n_e dl$$

We get a standard ruler: $A^2/E \simeq \Delta L$

If the structure of the gas is known, given the angular size ϑ of the system, the angular diameter distance, $D_A = \Delta L \backslash \vartheta$, is given by:

$$D_A(z) = A^2/(E\theta)$$

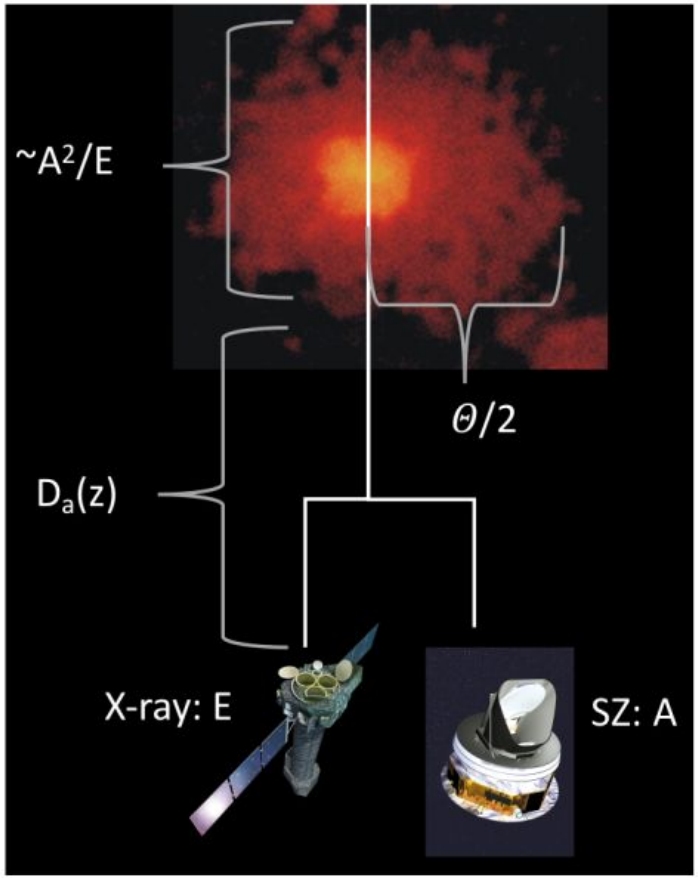

H_0 FROM X-RAY AND SZ MEASUREMENTS

- Birkinshaw (1979)
- Reese et al. (2000)
- Patel et al. (2000)
- Mason et al. (2001)
- Reese et al. (2002)
- Sereno (2003)
- Udomprasert et al. (2004)
- Reese et al. (2004)
- Schmidt et al. (2004)
- Jones et al. (2005)
- Bonamente et al. (2006)
- Kozmanyan et al. (2019)

SZ measurements from RT, OVRO and BIMA, X-ray from ROSAT
26 clusters z < 0.78
H_0 = 61±3(stat.)±18(sys.) km/s/Mpc

SZ measurements from OVRO, BIMA and X-ray from Chandra
38 clusters 0.14< z< 0.89
H_0 = 76.9±4(stat.) ±9(sys.) km/s/Mpc

Three regular clusters
z=0.088, 0.2523, and 0.451
H_0 = 68±8(stat.) km/s/Mpc

SZ measurments from Planck and X-ray from XMM
61 nearby systems (z<0.5)
H_0 = 67± 3km/s/Mpc

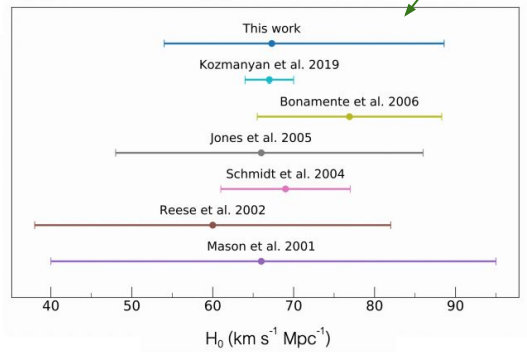

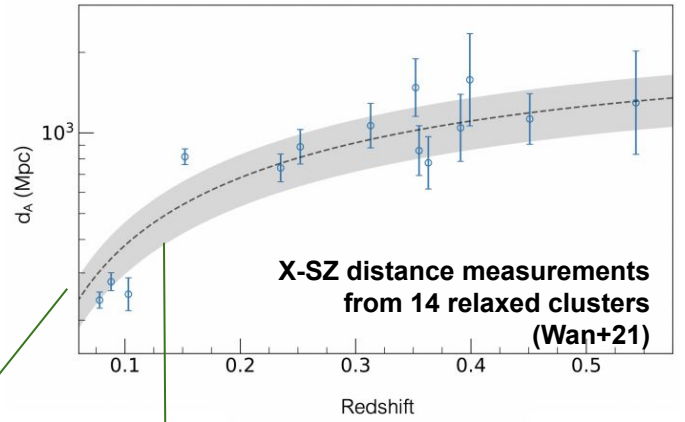

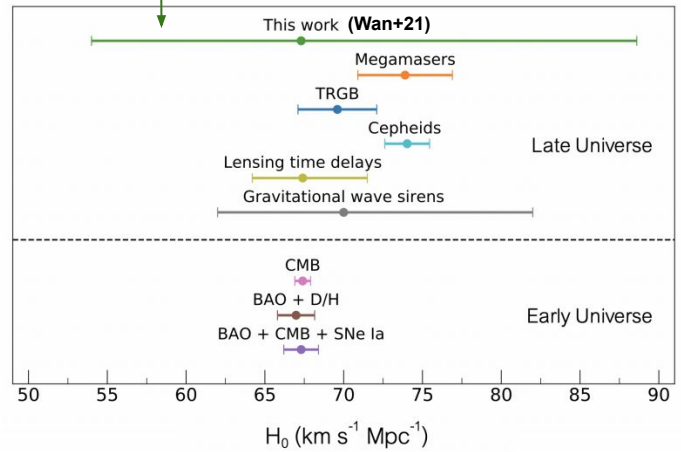

CMB SECONDARY ANISOTROPIES

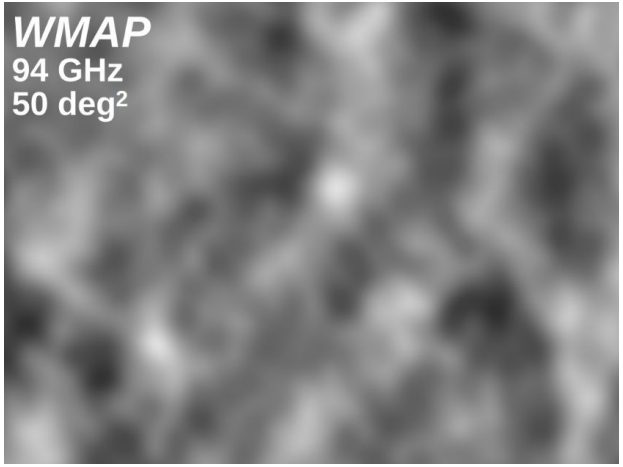

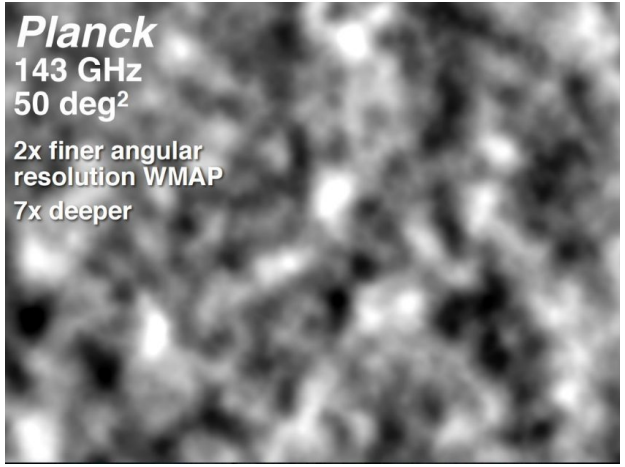

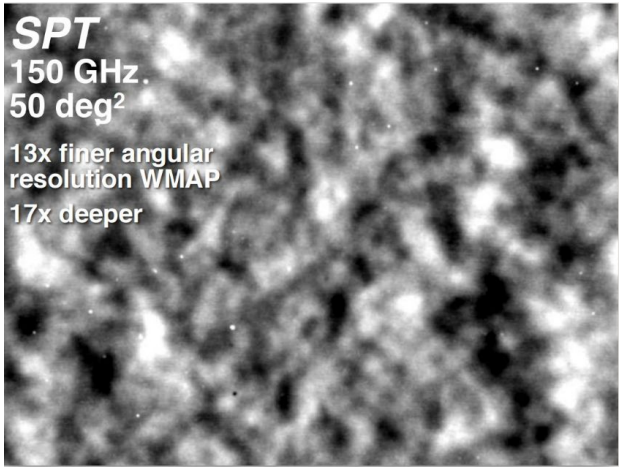

CMB SECONDARY ANISOTROPIES

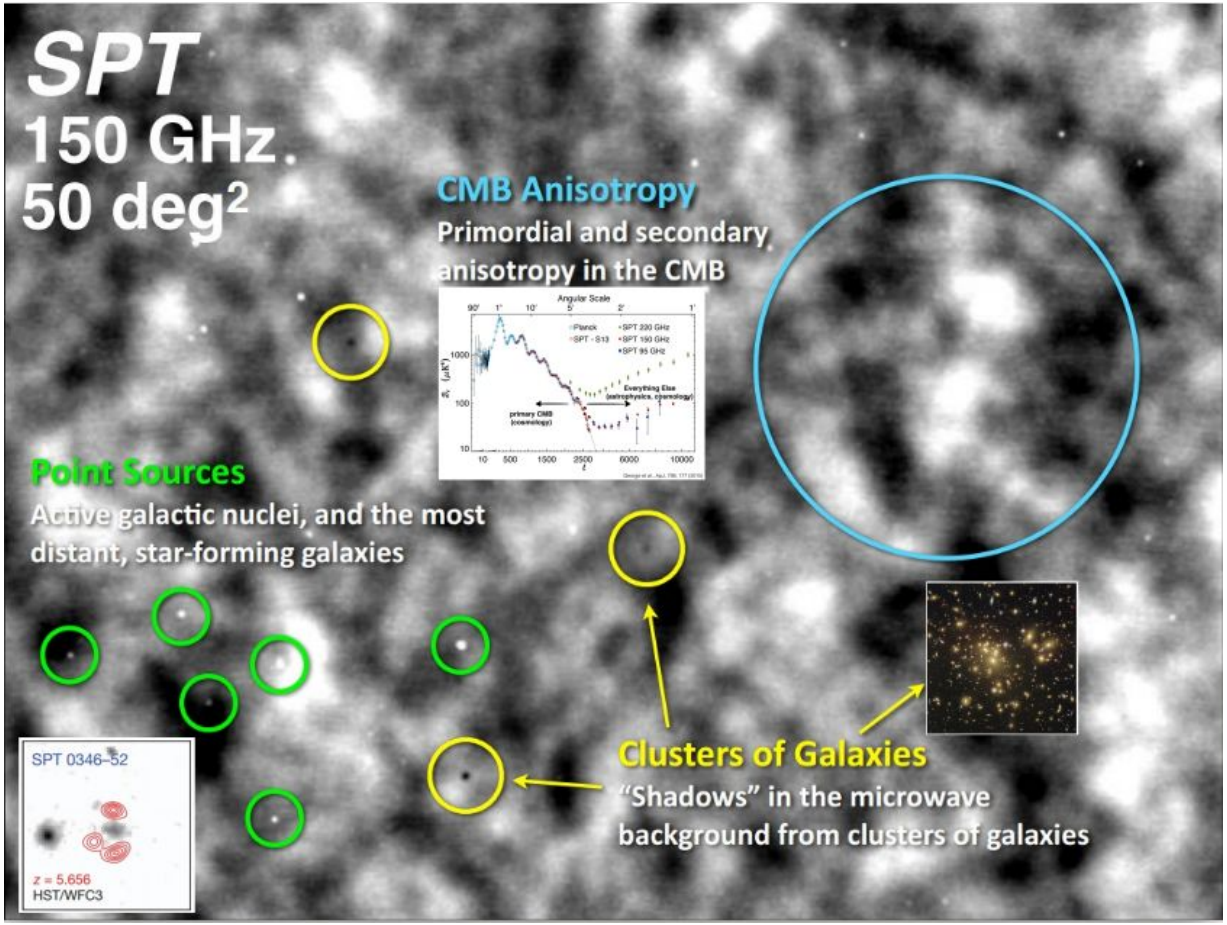

CMB SECONDARY ANISOTROPIES: tSZ

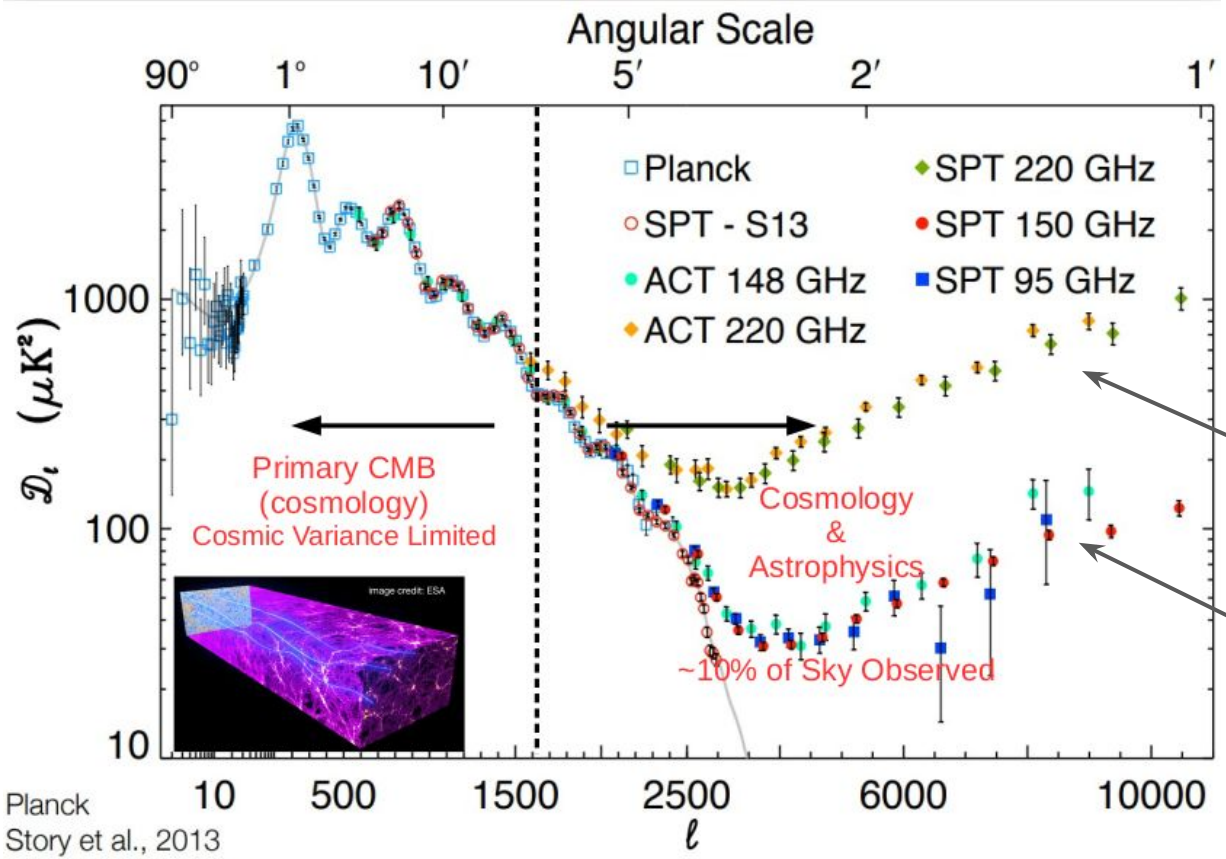

Planck
Story et al., 2013
George et al., 2014
Das et al., 2014

Signal at high multipole dominated by secondary anisotropies

Astrophysics becomes important to model the observed spectrum

@220 GHz: tSZ vanishes but there's contribution from CIB and radio point sources

@150 GHz: tSZ is negative, and dust is much dimmer than at 220 GHz

y-MAPS

$$\Delta T_i(\nu) = f(\nu) y_i + \mathrm{CMB}_i + \mathrm{Dust}_i + \mathrm{Noise}_i(\nu)$$

Table 1. Conversion factors for tSZ Compton parameter y to CMB temperature units and the FWHM of the beam of the *Planck* channel maps.

Frequency [GHz]	$T_{\mathrm{CMB}}\, g(\nu)$ [$\mathrm{K_{CMB}}$]	FWHM [arcmin]
100	−4.031	9.66
143	−2.785	7.27
217	0.187	5.01
353	6.205	4.86
545	14.455	4.84
857	26.335	4.63

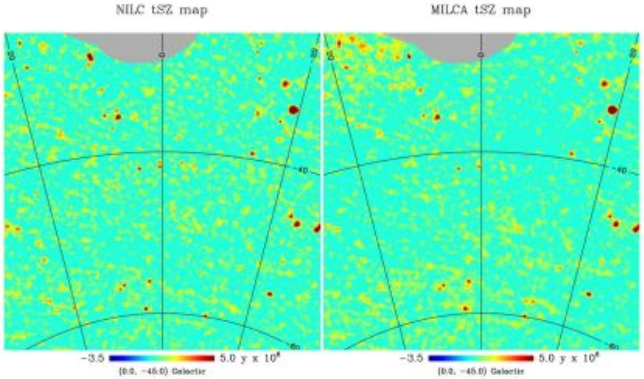

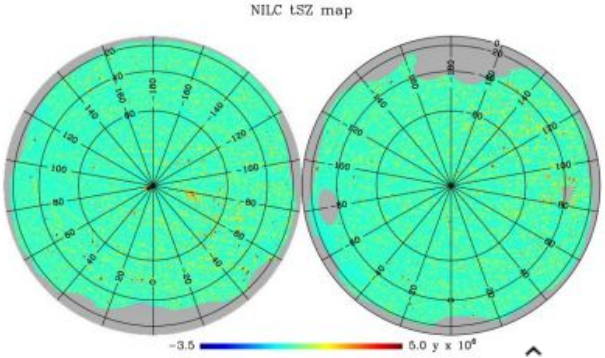

$$\hat{y}_i = \sum_\nu w_\nu \Delta T_i(\nu)$$

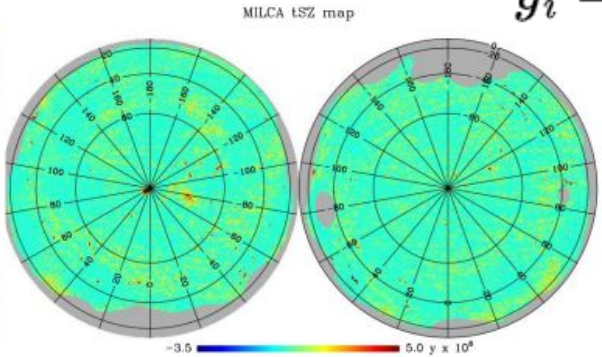

Planck 2013 results. XXI

y-MAPS

SPT 3G Compton-y map:

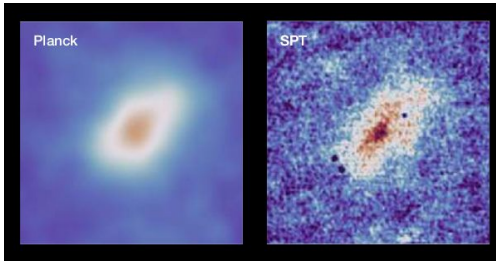

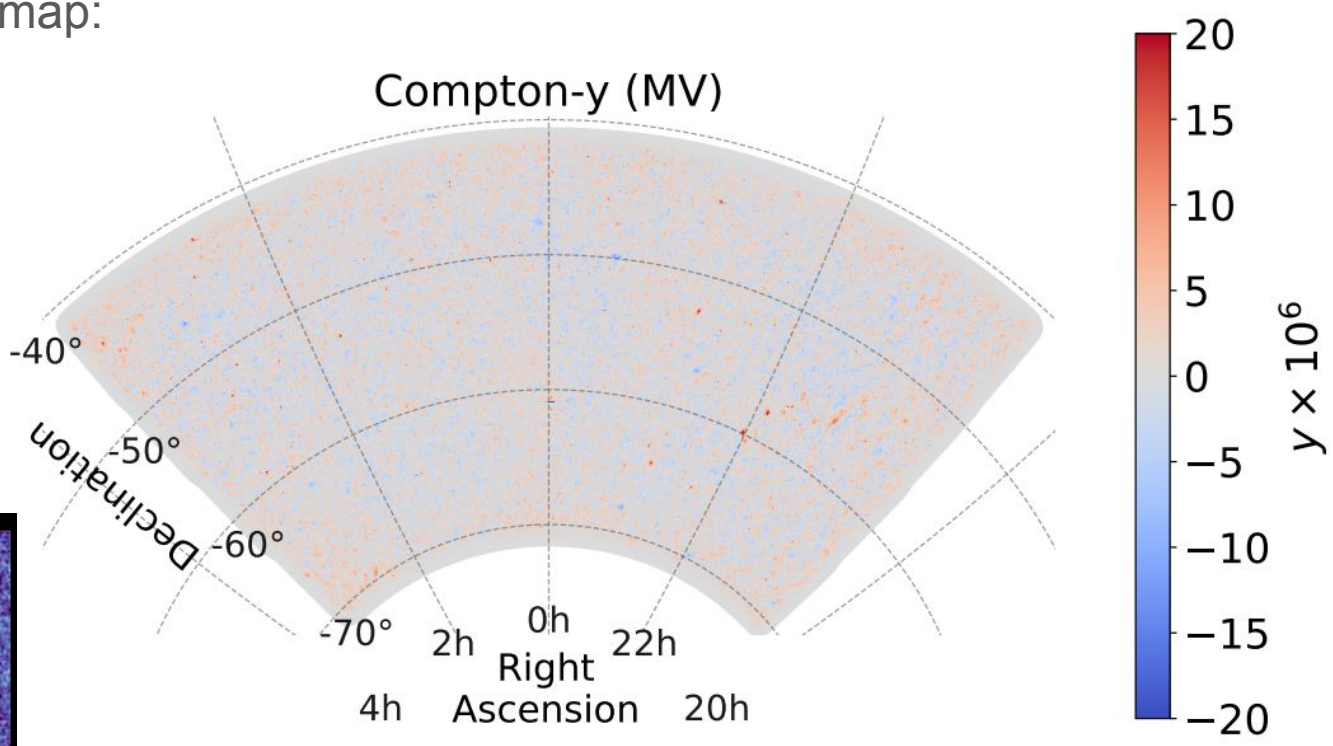

FIG. 2. The *Planck* and SPT-3G combined minimum-variance (MV) version of the Compton-y map provided with this work. We can see numerous galaxy clusters prominently visible as reddish features, resulting from the tSZ effect.

tSZ POWER SPECTRUM

Similarly to the CMB temperature anisotropies we can study the statistical properties of the y-map computing the angular power spectrum:

- **Expand in spherical harmonics:**

$$y(\boldsymbol{n}) = \sum_{\ell m} y_{\ell m}\, Y_{\ell m}(\boldsymbol{n})$$

- **Compute the angular power spectrum:**

$$C_\ell^{\mathrm{tSZ}} = \frac{1}{2\,\ell + 1} \sum_m y_{\ell m} y_{\ell m}^{*}.$$

tSZ POWER SPECTRUM

Even after cleaning process the y-maps is not free from contamination:

$$C_\ell^{\rm total} = C_\ell^{\rm tSZ} + C_\ell^{\rm CIB} + C_\ell^{\rm RS} + C_\ell^{\rm IR}$$

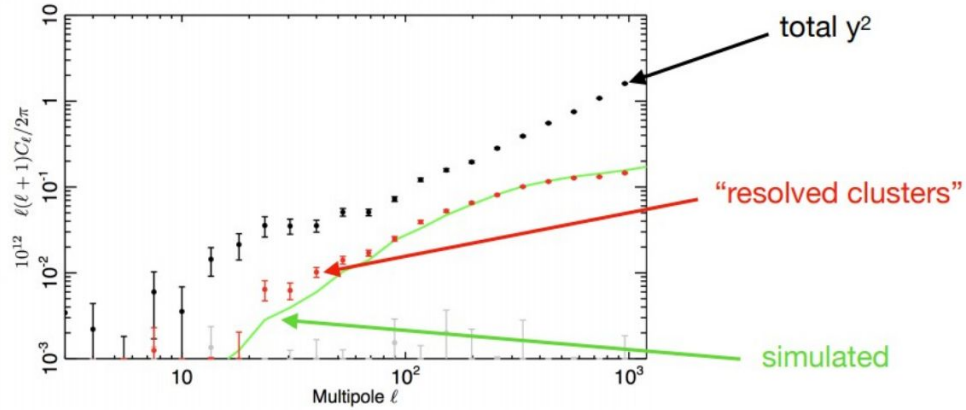

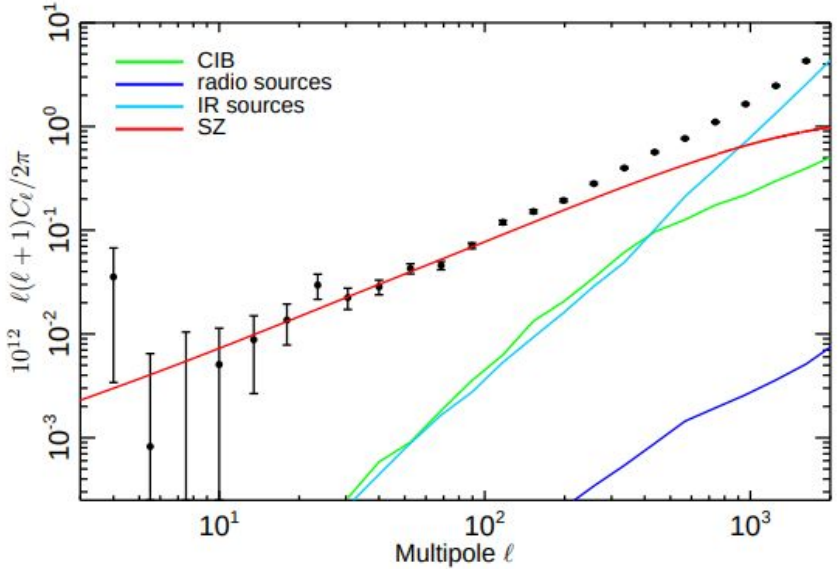

Fig. 15: NILC - MILCA F/L cross-power spectrum (black) compared to the power spectra of the physically motivated foreground models. The considered foregrounds are: clustered CIB (green line); infrared sources (cyan line); and radio sources (blue line). Additionally, the best-fit tSZ power spectrum model presented in Sect. 7.1 is also plotted as a solid red line.

Planck 2015 results

tSZ POWER SPECTRUM

Dependence on cosmological parameters:

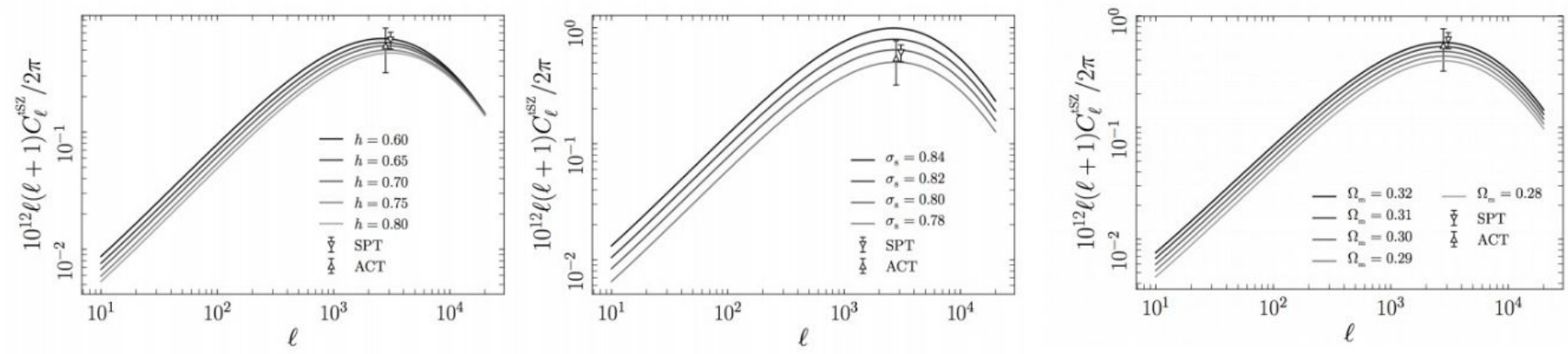

- **On large scale the amplitude scale as:**

$$C_\ell^{\rm tSZ} \propto \sigma_8^{8.1}\Omega_{\rm m}^{3.2}B^{-3.2}h^{-1.7}$$

B = hydrostatic mass bias

- **Due to large degeneracies we can actually constrain the parameter combination:**

$$F \equiv \sigma_8(\Omega_{\rm m}/B)^{0.40}h^{-0.21}$$

tSZ POWER SPECTRUM

Dependence on cosmological parameters: impact of hydrostatic mass bias

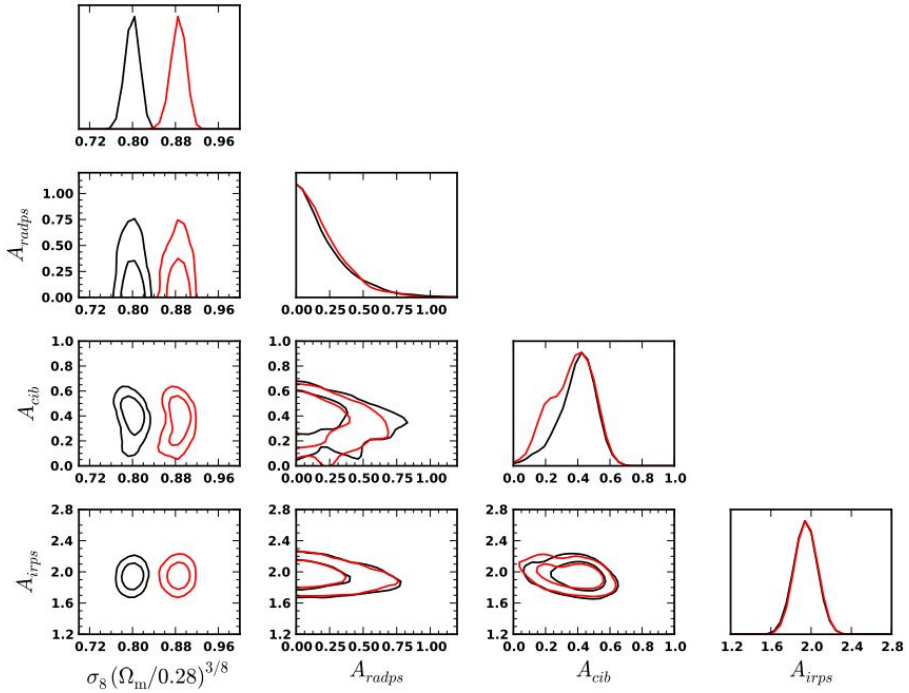

Planck 2015 results

Fig. 16: 2D and 1D likelihood distributions for the combination of cosmological parameters $\sigma_8(\Omega_{\rm m}/0.28)^{3/8}$, and for the foreground parameters $A_{\rm Rad.PS}$, $A_{\rm CIB}$ and $A_{\rm IR.PS}$. We show the 68.3% and 95.4% C.L. contours. The red and black contours correspond to a fixed mass bias of 0.2 and 0.4 respectively.

tSZ POWER SPECTRUM

Dependence on cosmological parameters:

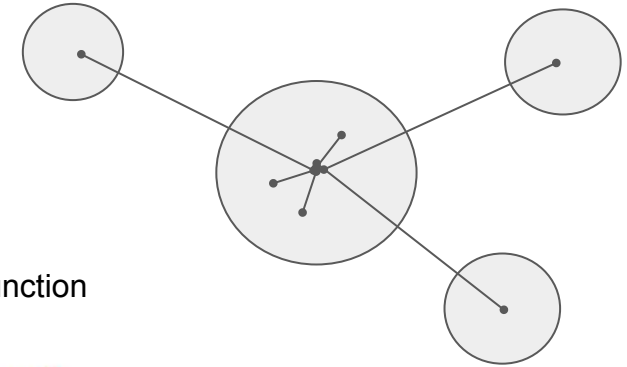

$$xC_\ell^{\rm SZ} = C_\ell^{\rm 1halo} + C_\ell^{\rm 2halos}$$

Halo mass function

$$C_\ell^{\rm 1halo} = \int_0^{z_{\rm max}} dz \frac{dV_{\rm c}}{dz d\Omega} \int_{M_{\rm min}}^{M_{\rm max}} dM \frac{dn(M,z)}{dM} |\tilde{y}_\ell(M,z)|^2$$

FT of radial compton-y profile of individual clusters

$$C_\ell^{\rm 2halos} = \int_0^{z_{\rm max}} dz \frac{dV_{\rm c}}{dz d\Omega} \times$$

Halo bias

$$\left[\int_{M_{\rm min}}^{M_{\rm max}} dM \frac{dn(M,z)}{dM} |\tilde{y}_\ell(M,z)| \; B(M,z) \right]^2 P(k,z)$$

Matter power spectrum

tSZ EFFECT: RELATIVISTIC CORRECTIONS

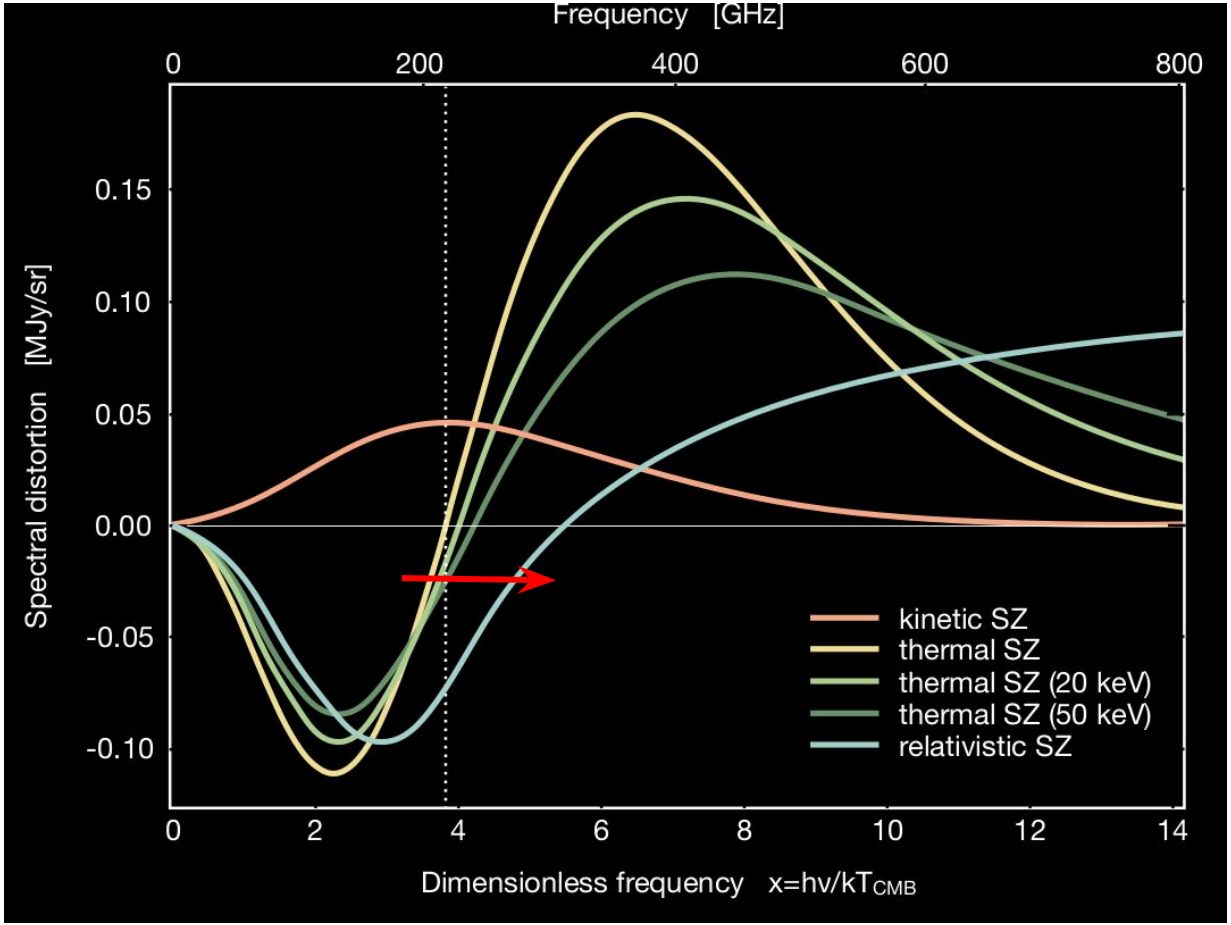

$$\Delta I_\nu = y \cdot I_0 \cdot [g(x) + \delta_{rel}(x, T_e)]$$

- **Relativistic corrections modify the zero frequency of the tSZ spectral distortion, that follows the relation $v_0 \simeq 217.4 + T_e/2$.**
- **Note also the significant increase of the 353 to 545 GHz tSZ intensity ratio.**
- **In general, higher temperatures for the plasma will favor a higher tSZ amplitude at high-frequencies, and a lower tSZ intensity at low frequencies.**

tSZ EFFECT: RELATIVISTIC CORRECTIONS

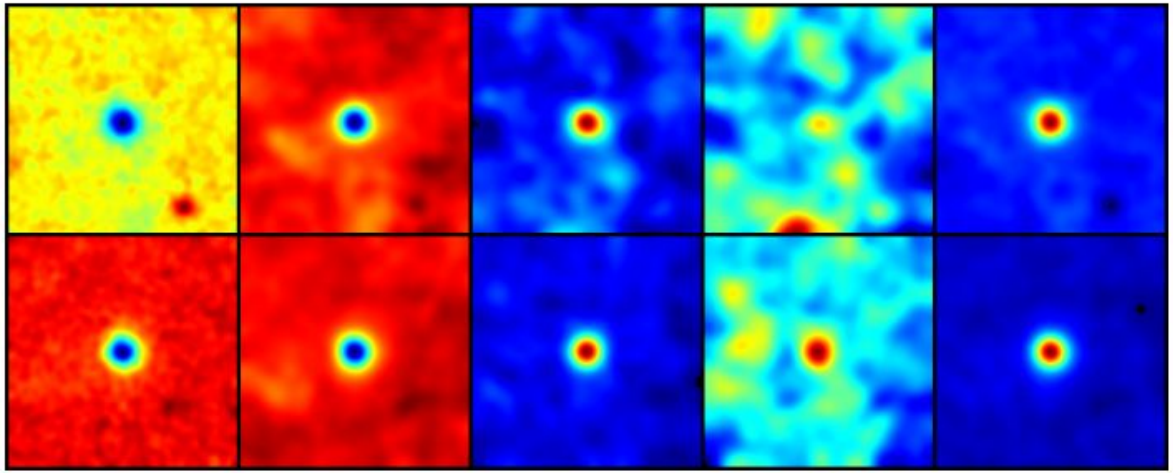

Figure 2. From left to right: stack of Planck intensity maps at 100, 143, 353, 545 GHz cleaned by the 857 and 217 GHz channel, and MILCA tSZ map, centered on the location of Planck MCXC clusters for a low-T_e bin (top panel) and a high-T_e bin (bottom panel). Each stacked map represents an area of $2° \times 2°$.

Significant amount of tSZ signal in the 545 GHz stacked map for the high-temperature bin, whereas the low-temperature bin does not present a significant tSZ emission at this frequency

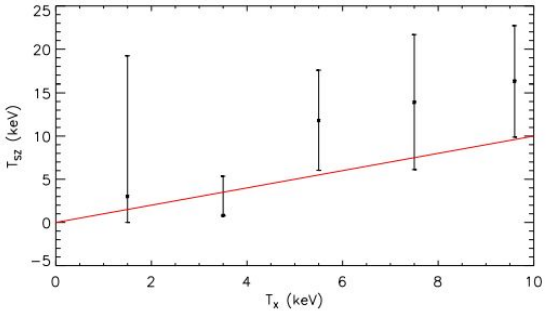

Figure 3. Measured temperature from tSZ relativistic correction for the MCXC galaxy cluster sample, as a function of the temperature derived from X-ray luminosity. The 1:1 relation is shown as a solid red line.

Hurier et al. 2017 (https://arxiv.org/pdf/1701.09020)

kSZ EFFECT

Kinematic Sunyaev-Zel'dovich effect: secondary anisotropy of the CMB caused by the bulk motion of free electrons (typically in the ICM):

- **CMB photons scatter off free electrons via Thomson scattering. If the electrons have a peculiar velocity v_{pec} along the line of sight, the scattered photons experience a Doppler shift which produces a temperature fluctuation**

$$\Delta T_{kSZ} = -T_{CMB} \int n_e \sigma_T \frac{\vec{v}\cdot\hat{n}}{c} dl = -T_{CMB} \left(\frac{v_{pec}}{c}\right) \tau_e$$

- **Unlike the tSZ, the kSZ does not change the shape of the CMB spectrum – frequency independent (to first order) – but it simply shifts the temperature**
- **It is much weaker than the tSZ (typically by a factor of 10, $\Delta T/T \sim 10^{-6}$)**
- **Unique tool for measuring the peculiar velocities of clusters, and direct probe of large-scale velocity field**

kSZ EFFECT

Pairwise kSZ: Since the kSZ signal from a single cluster is noisy and small we can stack pair of clusters, which on average, are infalling toward each other

Soergel et al. (2016)
4.2 sigma detection with ~6700 clusters

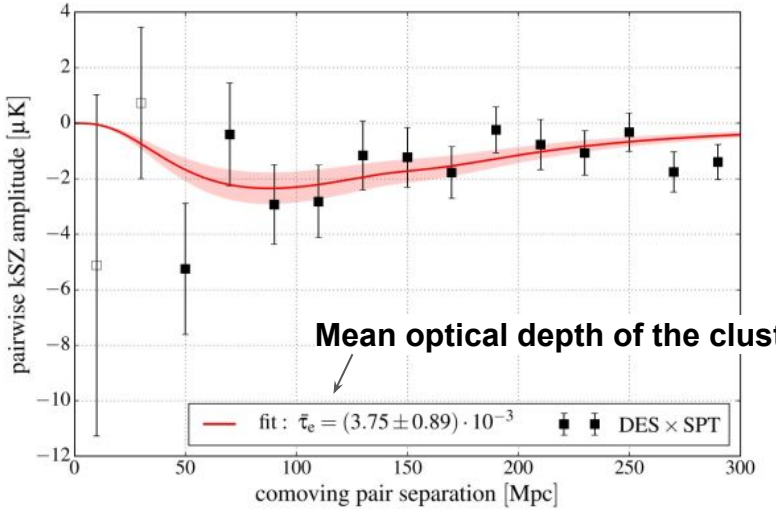

Figure 7. Pairwise kSZ amplitude measured from the DES Y1 redMaPPer catalogue and the SPT-SZ temperature maps, using the baseline sample of clusters with $20 < \bar{\lambda} < 60$. The solid red line shows the analytic pairwise velocity template (equation 11) scaled with the best-fitting optical depth $\bar{\tau}_e$; the shaded regions are the corresponding 1σ uncertainties. As before, the two lowest separation points shown with empty symbols are excluded from the fit, as on these scales perturbation theory is not valid.

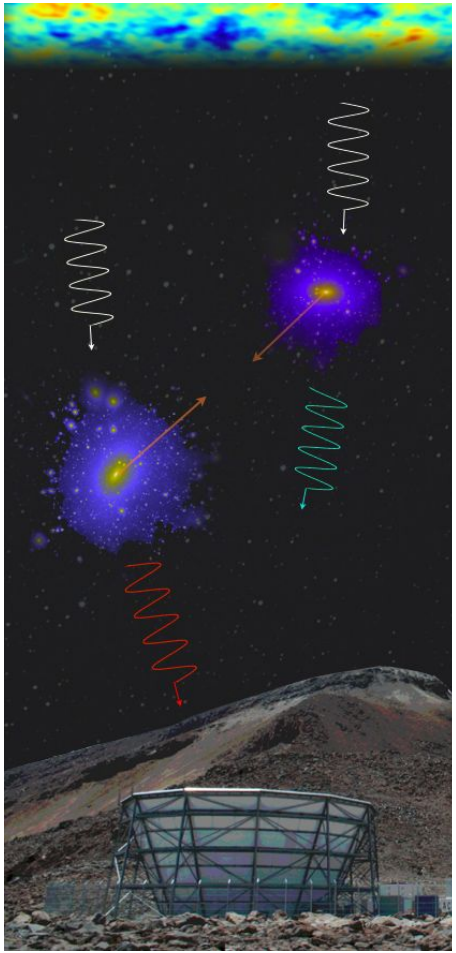

kSZ EFFECT

Rotating kSZ (Yang et al 2026):

- **Estimate the direction of the projected angular momentum by measuring the redshift dipole of satellite galaxies around their group centre**
- **Oriented stacking of the Planck CMB temperature map using the group centres and directions of angular momenta**
- **2.3σ measurement of the coherent rotational kSZ effect within the virial radii of SDSS groups with an average mass of $10^{14}\ h^{-1}M_{\odot}$**

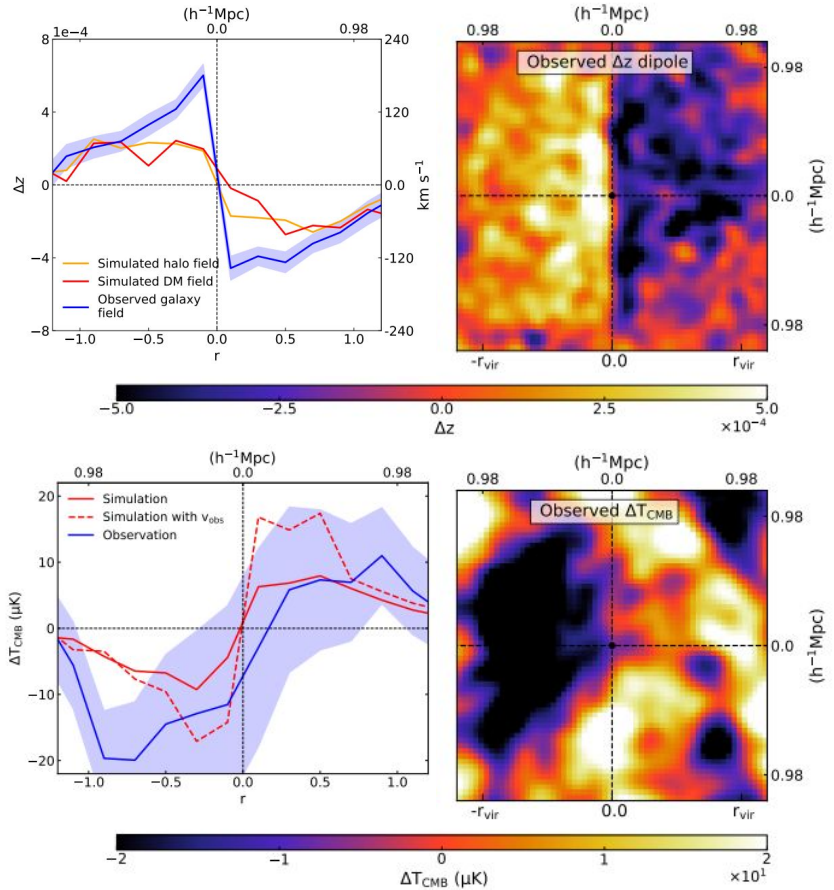

https://arxiv.org/pdf/2603.14494

SZ VIEW OF GALAXY CLUSTERS

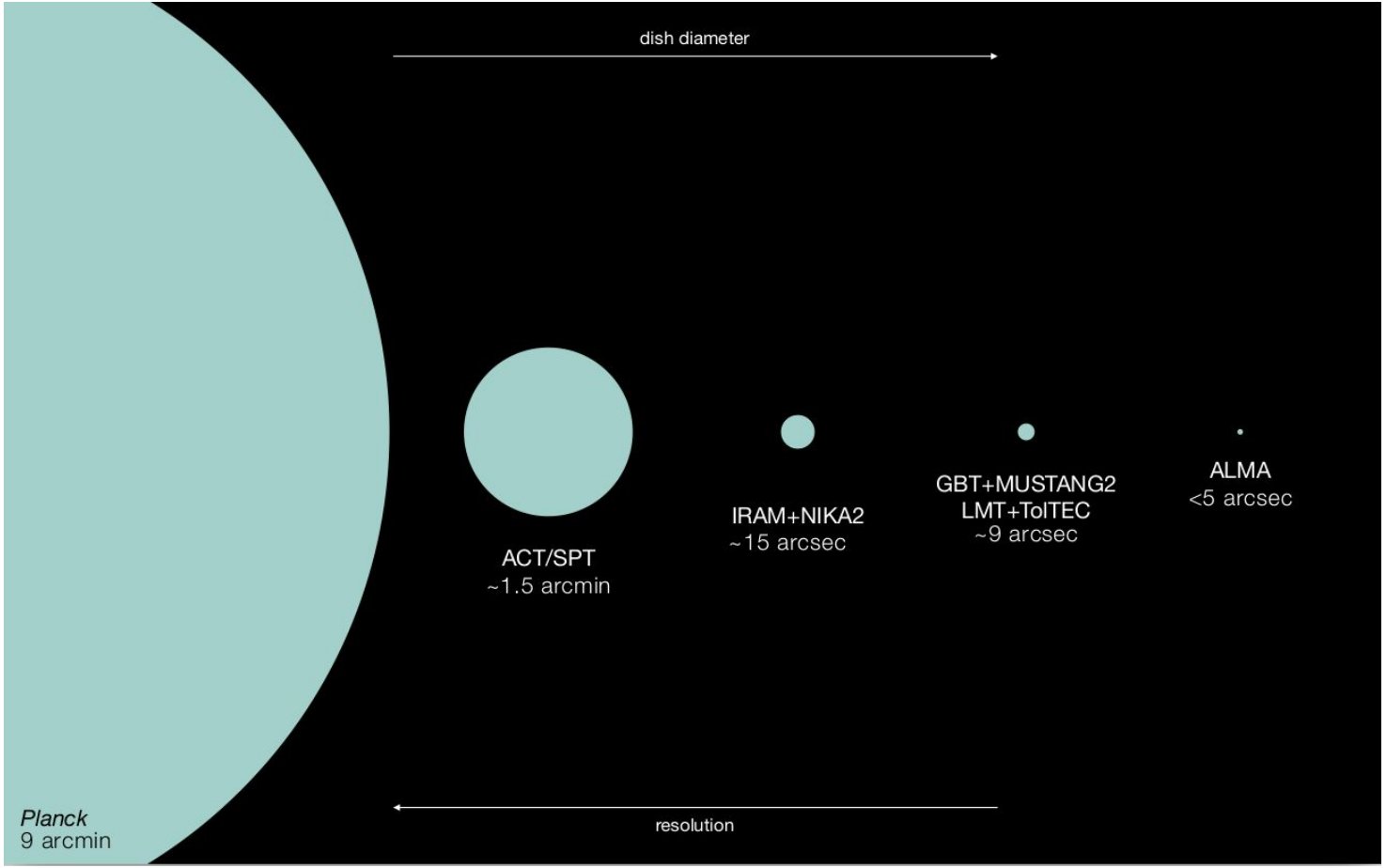

SZ VIEW OF GALAXY CLUSTERS

Planck's view of galaxy clusters

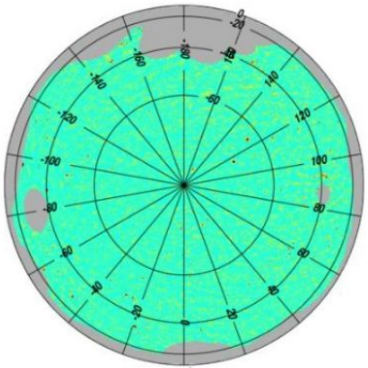

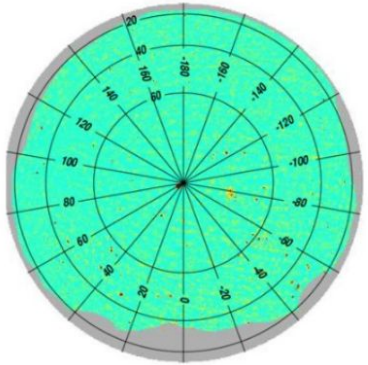

Adapted from Planck 2015 XXII

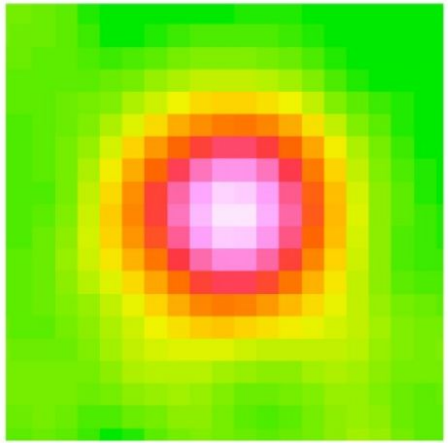

Planck Legacy Archive

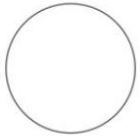

10 arcmin

SZ VIEW OF GALAXY CLUSTERS

Planck's view of galaxy clusters

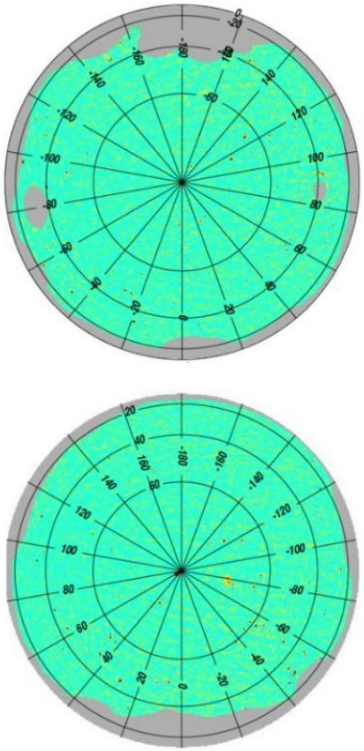

Adapted from Planck 2015 XXII

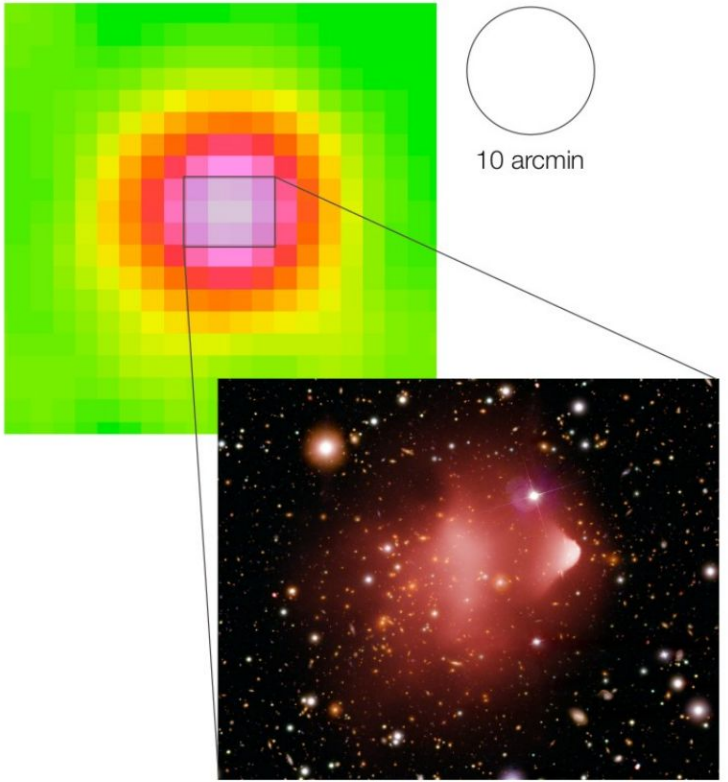

Chandra+HST

SZ VIEW OF GALAXY CLUSTERS

SPT-CL J2106 - 5844

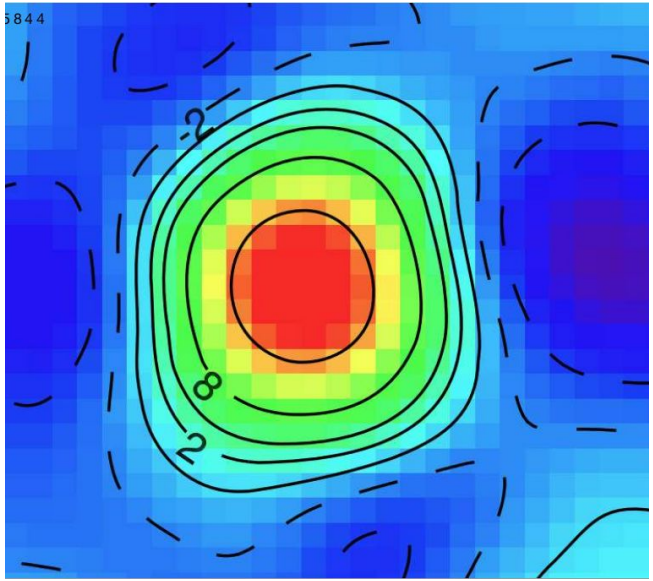

$z = 1.13$ $M = 10^{15} M_{\odot}$

Train Wreck (Abel 520)

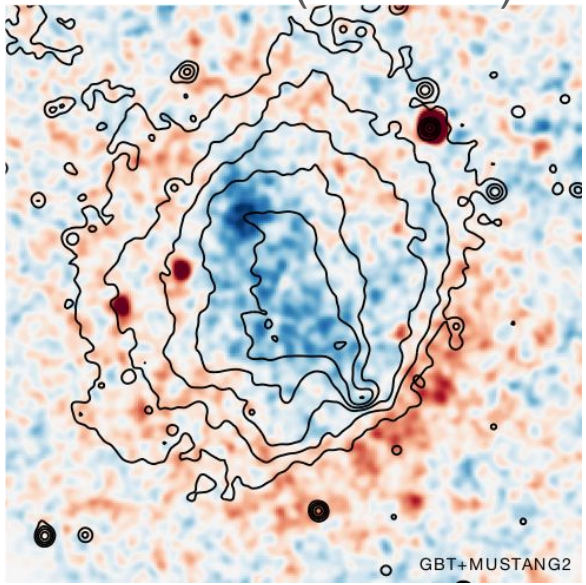

$z = 0.2$

Moo J1142+1527

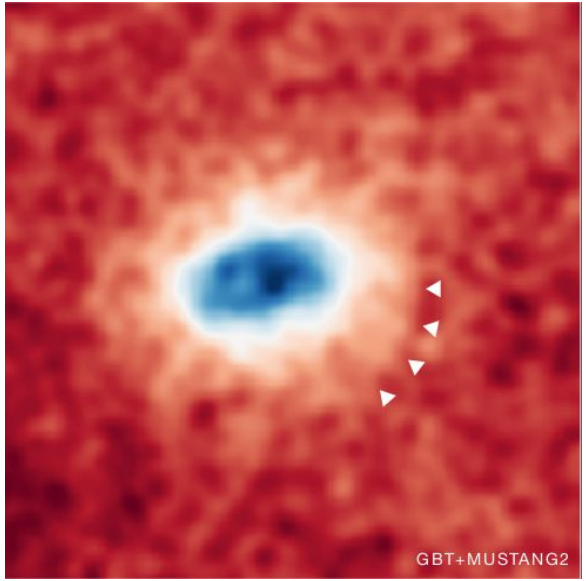

$z = 1.9$ $M = 1.1 \times 10^{15} M_{\odot}$

SZ CLUSTER CATALOGS

Optimal Matched Filter (Melin et al. 2006):

- **For each frequency map we have:**

$$\Delta T_i(\vec{\theta}) = y_0 S(\vec{\theta}) \cdot f(\nu_i) + \mathrm{Noise}_i(\vec{\theta})$$

Primary CMB
Astrophysical foregrounds
Instrumental noise

f(ν) = spectral dependence (tSZ frequency law)

$$S(\vec{\theta}) = \Delta T_0 (1 + |\vec{\theta}|^2/\theta_c^2)^{-1}$$

- **Matching the data to a template of what a cluster is expected to look like in both space (its shape) and frequency (its SZ signature)**
- **The filter ψ(k) is designed to maximize the Signal-to-Noise Ratio at the cluster's location**

$$\psi(\vec{k}) = \frac{B(\vec{k})S(|\vec{k}|)}{B(\vec{k})^2 N_{astro}(|\vec{k}|) + N_{noise}(\vec{k})}$$

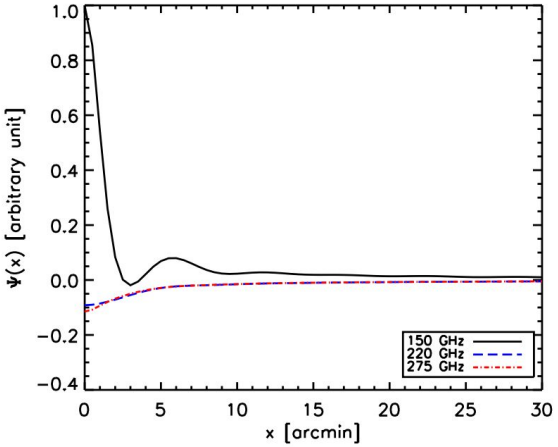

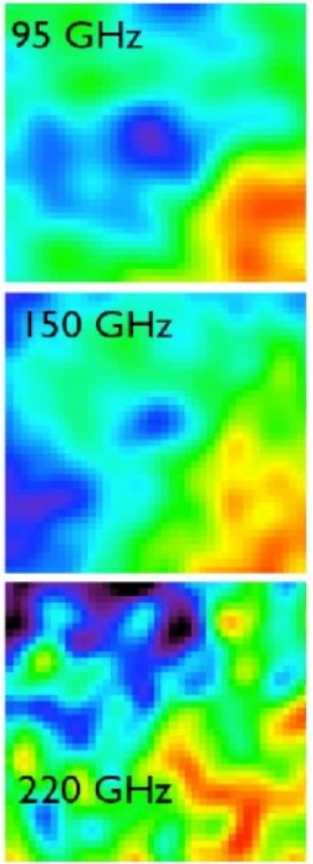

SZ CLUSTER CATALOGS

Optimal Matched Filter:

- **By combining channels is possible to "subtract" the primary CMB and noise away exploiting the spectral signature of the tSZ effect**
- **Detection: peaks in the filtered map above some S/N threshold**

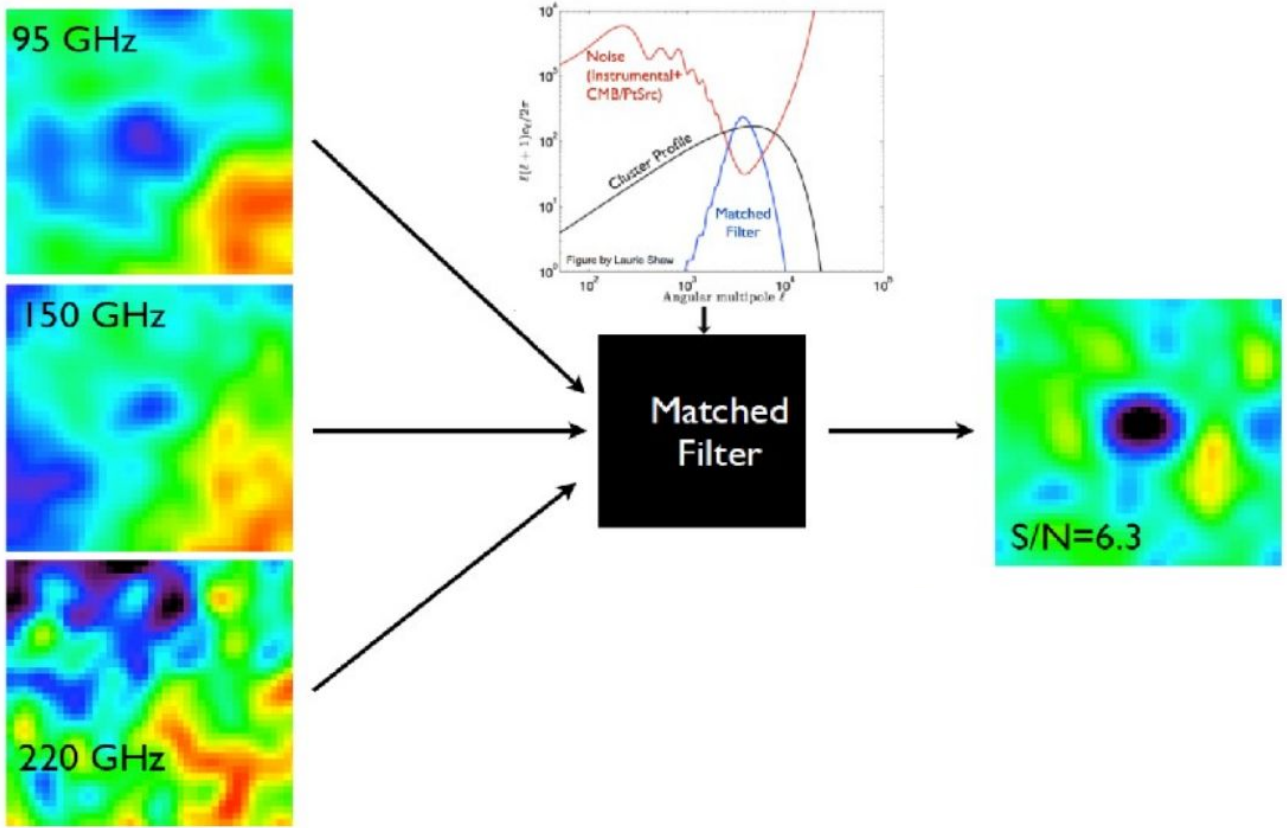

SZ CLUSTER CATALOGS

Optimal Matched Filter:

- **The actual size of the cluster is known →the filter is run multiple times assuming different spatial filter scales ϑ_c.**
- **For each scale compute S/N and select the scale maximizing the signal**

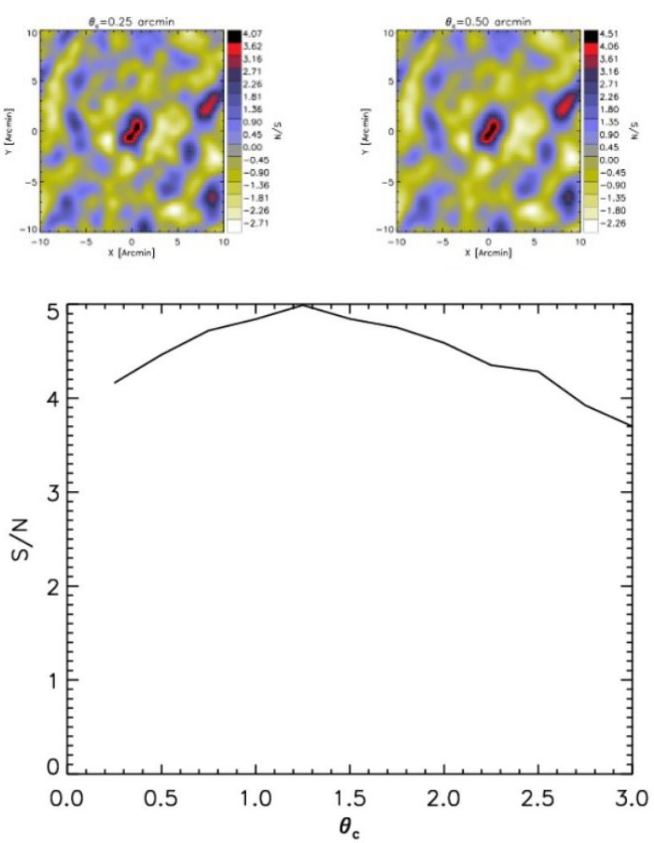

SZ CLUSTER CATALOGS

Staniszewski et al. 2009: First “blind” detection of SZ clusters using SPT data

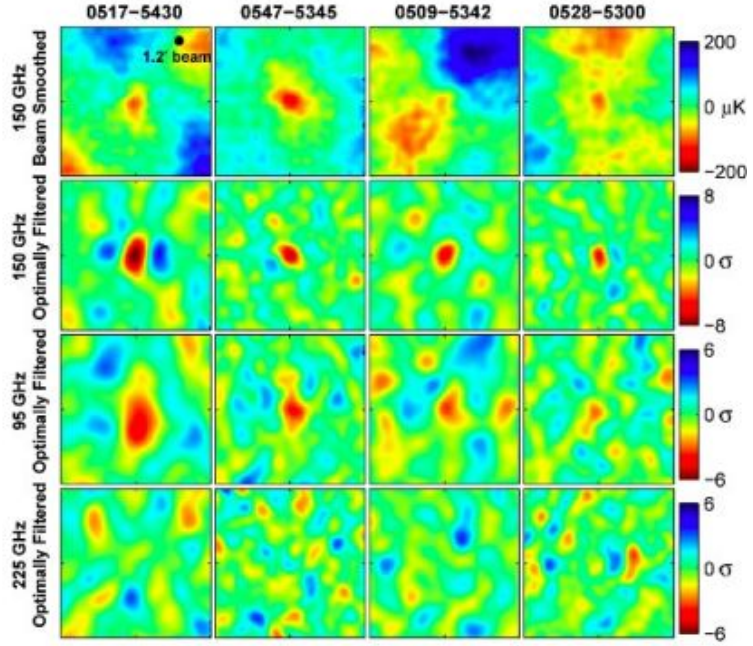

FIG. 1.— Images of four galaxy clusters found in the SPT SZ survey. In each panel, the region shown is a 20 by 20 arcmin box centered on the cluster. All images are oriented with north up and east to the left. In the top row, we show the beam-smoothed 150 GHz map, and the scale has units of μK_{CMB}. The lower three rows show the 150, 95 and 225 GHz maps filtered using a $\beta = 1$ model with the θ_{core} listed in Table 1. The ringing on either side

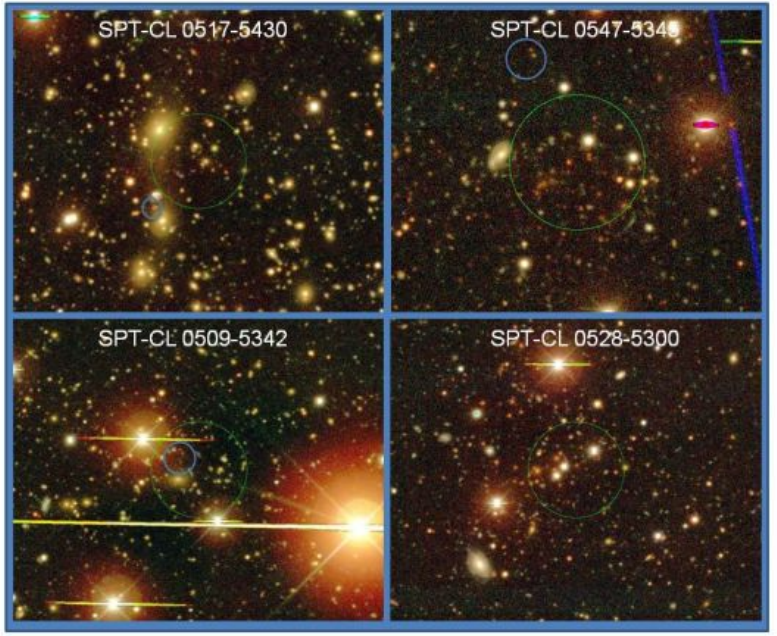

SZ CLUSTER CATALOGS

SZ cluster candidate confirmation:

- **The SZ signal is noisy and redshift independent → Optical and NIR follow up data needed to confirm the detection, and assign a redshift to the cluster**

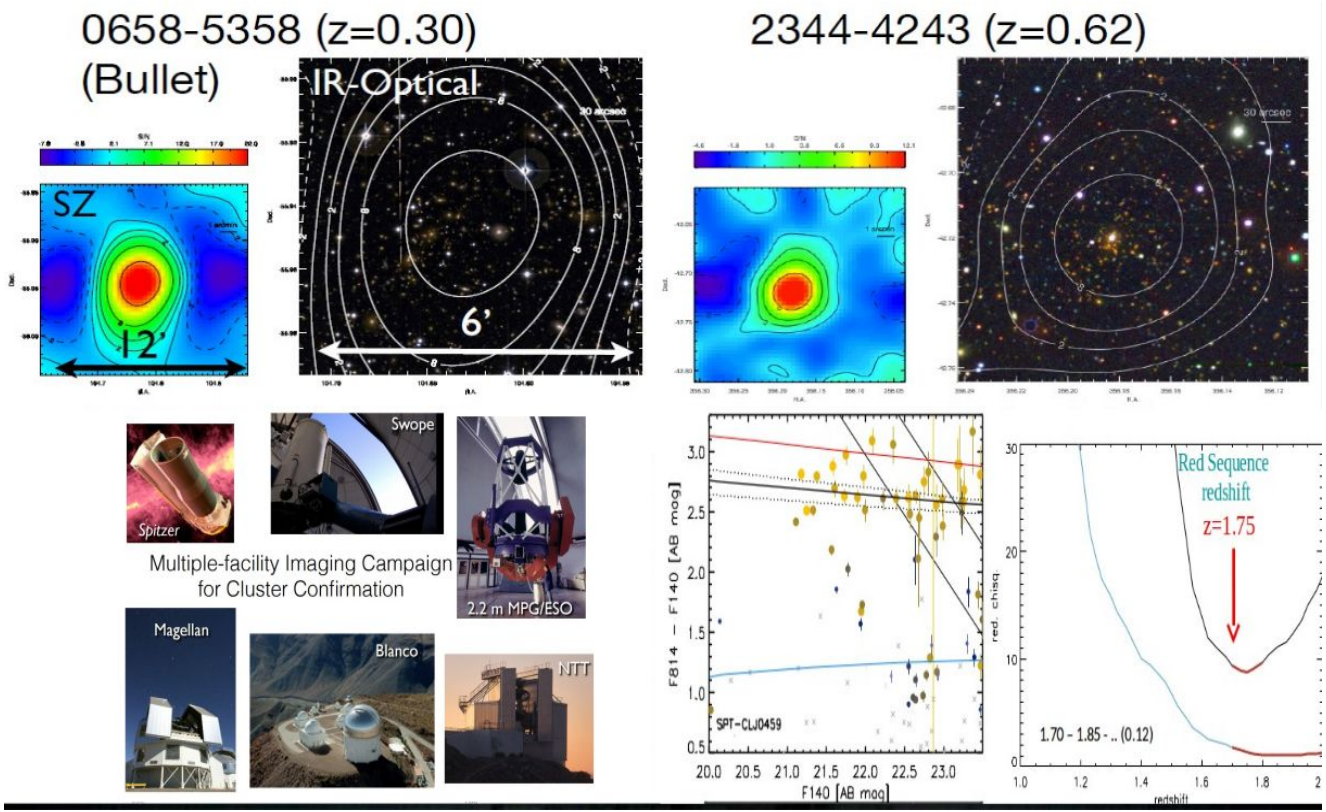

SZ CLUSTER CATALOGS

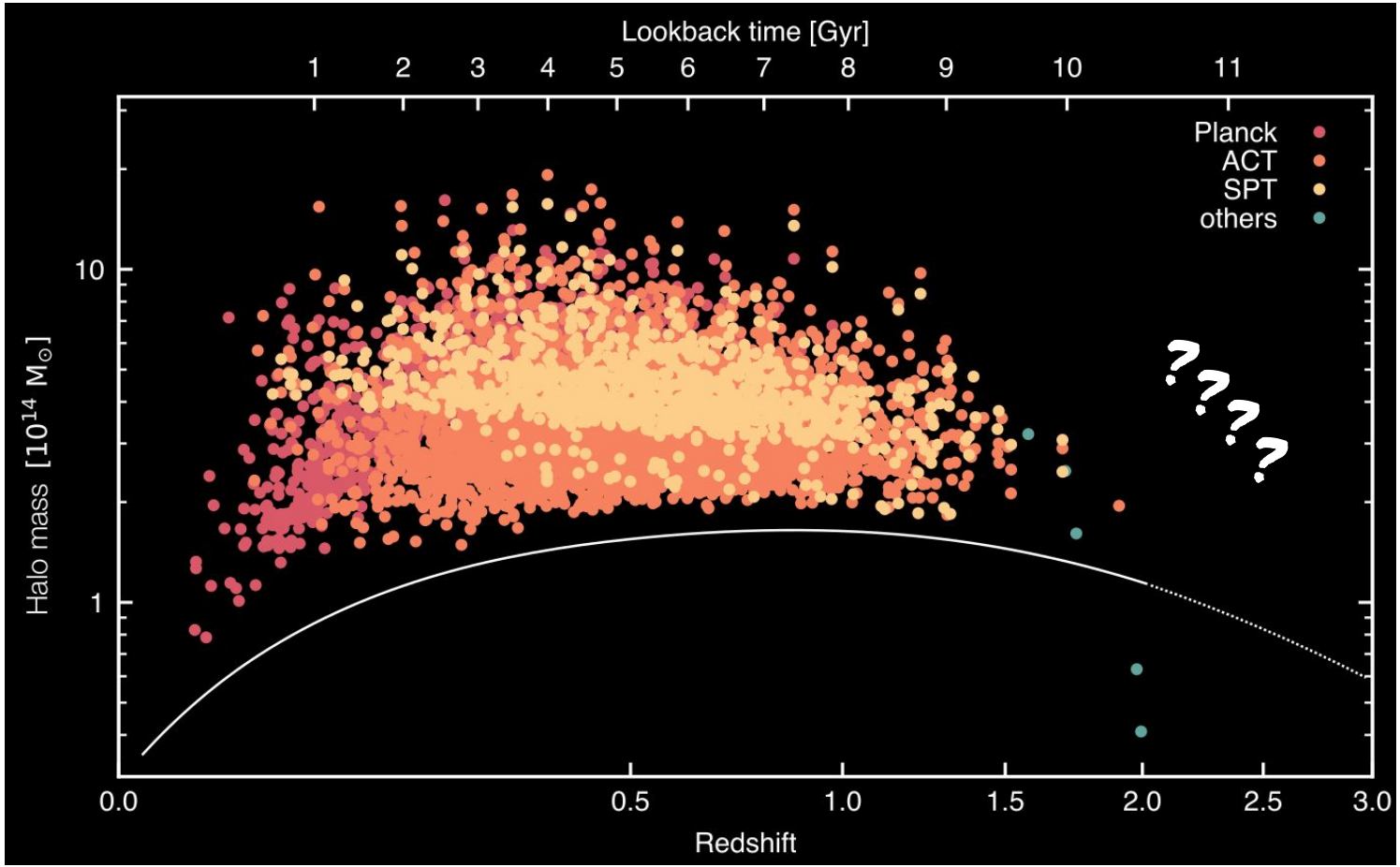

PROTOCLUSTER

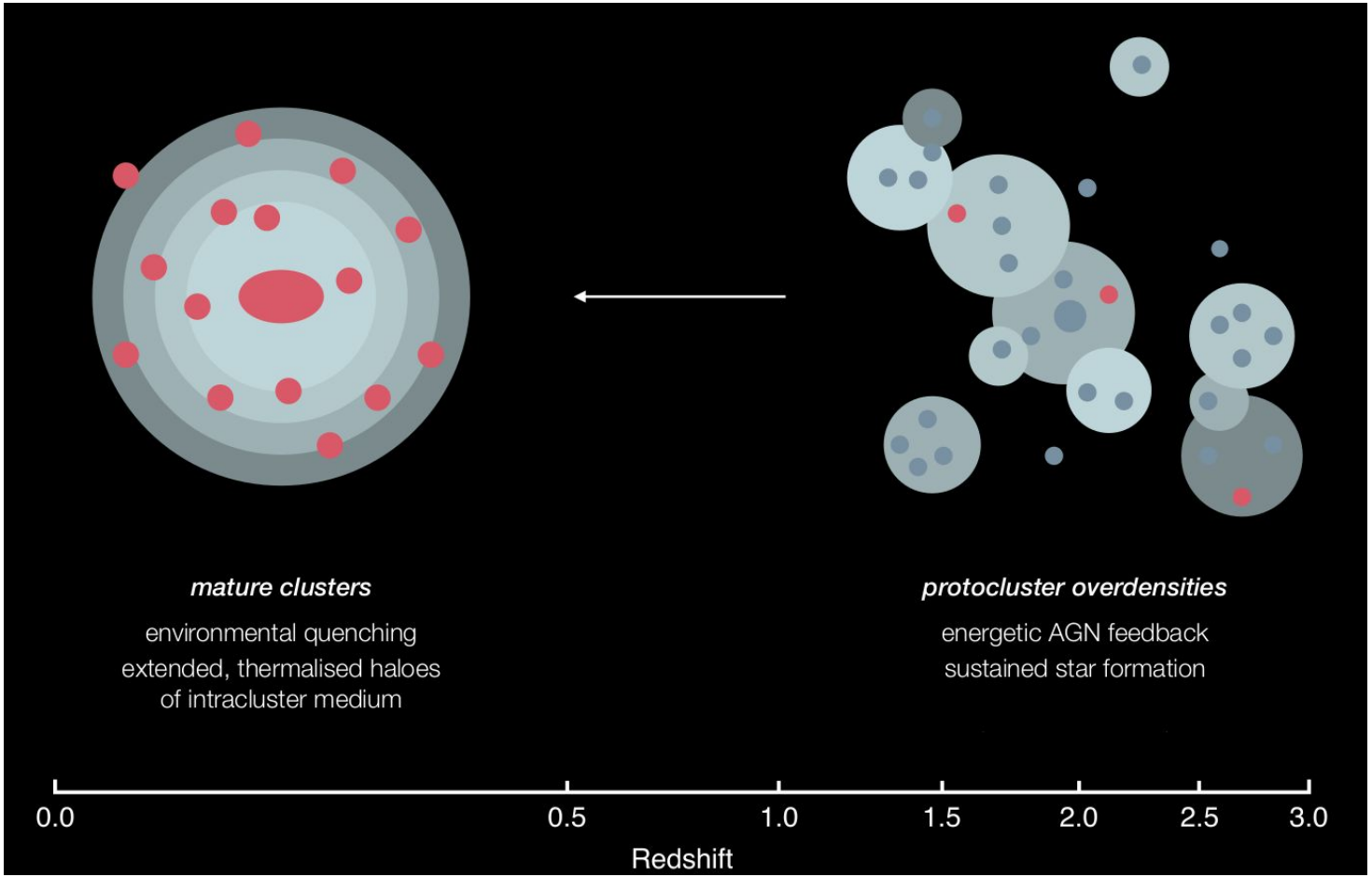

PROTOCLUSTER

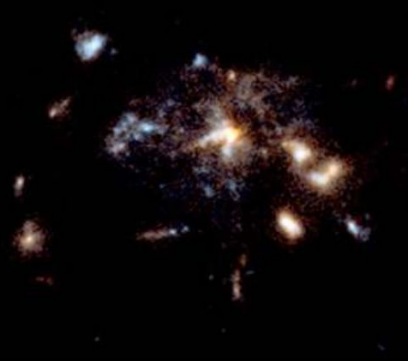

Pentericci+1997, Hatch+2009
Star-bursting proto-BCG fed by "cooling flow"-like precipitation (but not the only scenario)

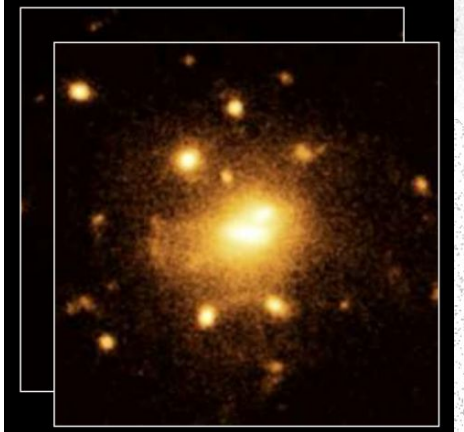

Saro+2009
simulated protoclusters with gravitational potential permeated by ICM at 2-5 keV

700ks Chandra observation of Spiderweb

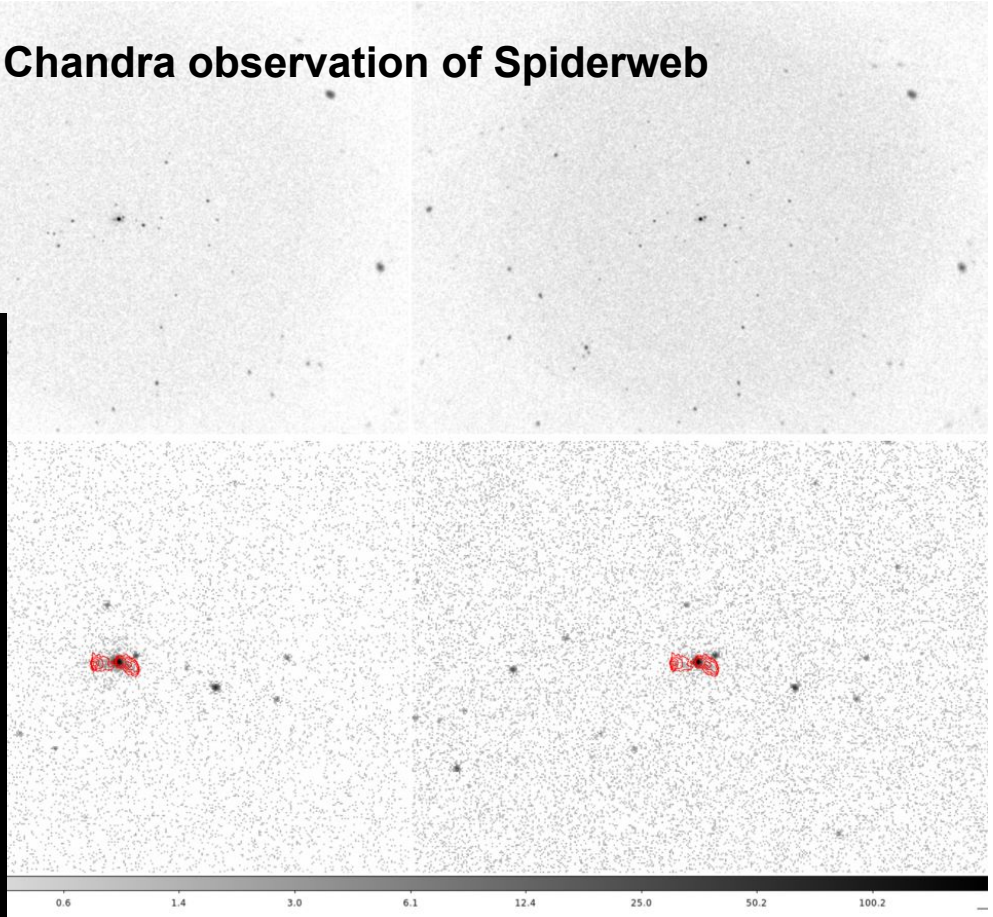

PROTOCLUSTER

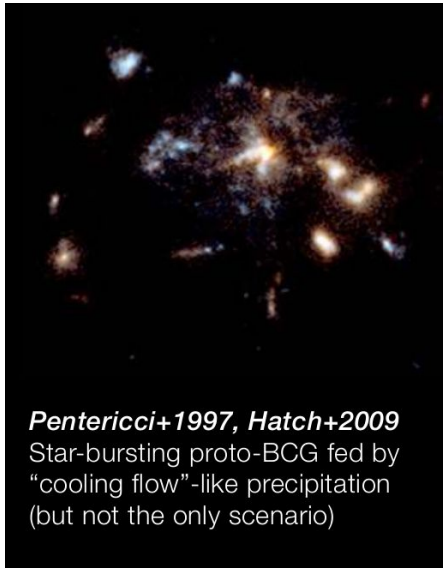

Pentericci+1997, Hatch+2009
Star-bursting proto-BCG fed by "cooling flow"-like precipitation (but not the only scenario)

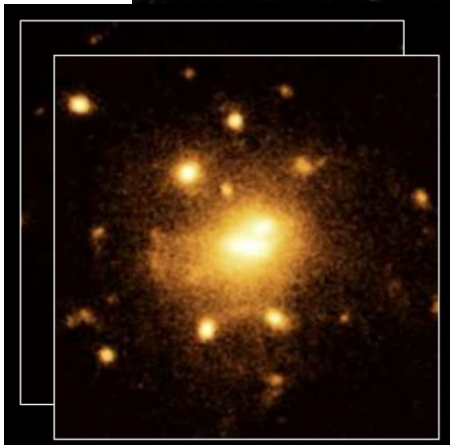

Saro+2009
simulated protoclusters with gravitational potential permeated by ICM at 2-5 keV